Regionally optimized high resolution input datasets enhance the representation of snow cover in CLM5

Johanna Teresa Malle[1,2], Giulia Mazzotti[2,3], Dirk Nikolaus Karger[1+], and Tobias Jonas[2+]

[1]Swiss Federal Research Institute for Forest, Snow, and Landscape Research (WSL), Zürcherstrasse 111, 8903, Birmensdorf, Switzerland
[2]WSL Institute for Snow and Avalanche Research SLF, Davos Dorf, Switzerland
[3]Univ. Grenoble Alpes, Université de Toulouse, Météo-France, CNRS, CNRM, Centre d'Études de la Neige, 38100 St. Martin d'Hères, France
[*]These authors contributed equally to this work.

Correspondence: Johanna Malle (johanna.malle@wsl.ch)

Abstract. Land surface processes, crucial for exchanging carbon, nitrogen, water, and energy between the atmosphere and terrestrial Earth, significantly impact the climate system. Many of these processes vary considerably at small spatial and temporal scales, in particular in mountainous terrain and complex topography. To examine the impact of spatial resolution and representativeness of input data on modeled land surface processes, we conducted simulations using the Community Land
5   Model 5 (CLM5) at different resolutions and based on a range of input datasets over the spatial extent of Switzerland. Using high-resolution meteorological forcing and land-use data, we found that increased resolution substantially improved the representation of snow cover in CLM5 (up to 52% enhancement), allowing CLM5 to closely match performance of a dedicated snow model. However, a simple lapse-rate based temperature downscaling provided large positive effects on model performance, even if simulations were based on coarse-resolution forcing datasets, only. Results demonstrate the need for resolutions
10   higher than 0.25°for accurate snow simulations in topographically complex terrain. These findings have profound implications for climate impact studies. As improvements were observed across the cascade of dependencies in the land surface model, high spatial resolution as well as high-quality forcing data becomes necessary for accurately capturing the effects of a reclining snowcover and consequent shifts in the vegetation period, particularly in mountainous regions. This study further highlights the utility of multi-resolution modeling experiments when aiming to improve representation of variables in land surface models.
15   By embracing high-resolution modeling, we can enhance our understanding of the land surface and its response to climate change.

1   Introduction

The Earth's changing climate is causing profound alterations in ecosystems globally, with large impacts on ecological, hydrological, and climatological processes (Pachauri et al., 2014; IPCC, 2022). In the context of the climate system, land surface
20   processes control the exchange of carbon, nitrogen, water and energy between the atmosphere and terrestrial ecosystems, hence profoundly influencing contemporary and future climate dynamics (Ferguson et al., 2012; Dirmeyer et al., 2006; Seneviratne

et al., 2006). Seasonal snow cover greatly impacts this complex interplay, as it plays a vital role in the Earth's energy balance and hydrological cycle (Flanner and Zender, 2005; Barnett et al., 2005). More specifically, snow's characteristic high reflectivity (Flanner et al., 2011) substantially modulates land surface albedo and energy balance, while its low thermal conductivity (Zhang, 2005) allows snow to act as an insulating blanket for soil and organisms. More generally, agricultural irrigation often heavily relies on snow-melt for food production (Qin et al., 2020), while more than one sixth of the world's population is dependent on water from glaciers or snow melt (Barnett et al., 2005), highlighting the importance of glaciers and snow for human water demand (Mankin et al., 2015; Pritchard, 2019).

Within the integrated Earth System, important interactions and feedback mechanisms exist between energy, water, and nutrient cycles. In seasonally snow-covered areas, the snowpack creates numerous such interactions: it influences the energy balance by modulating the exchange of heat and moisture between the land surface and the atmosphere (Thackeray et al., 2019). It influences the partitioning of energy fluxes, affecting the magnitudes of both sensible and latent heat fluxes (Male and Granger, 1981), which, in turn, regulate the transfer of energy and water vapor, shaping the local and regional climate patterns (Ban-Weiss et al., 2011). Moreover, the duration and extent of snow cover has direct implications for vegetation periods, which has the potential to impact gross primary production (GPP), a measure of vegetation's ability to convert solar energy into chemical energy (and carbon dioxide to organic matter) through photosynthesis (Slatyer et al., 2022). Therefore, the presence or absence of snow cover directly influences the availability of water and sunlight for plants, influencing the productivity and carbon cycling within terrestrial ecosystems and resulting in direct links between melt-out date and biomass production (Jonas et al., 2008).

The Global Climate Observing System (GCOS, https://gcos.wmo.int/) has identified Snow Cover Extent as an essential climate variable, which further underlines the importance of snow for monitoring climate change and the critical role it has in regulating the energy balance of the planet. In physically-based models, the representation of seasonal snow and its evolution are usually based on mass- and energy balance calculations. Representations of snowpack structure range from simple, one-layer approaches (Douville et al., 1995) to complex schemes that resolve up to 50 snowpack layers and track the evolution of their microstructural properties (Vionnet et al., 2012; Bartelt and Lehning, 2002). For model applications at large scales and coarse resolutions, snowpack representations with few (3 to ca. 10) layers (Essery et al., 2013; Niu et al., 2011) have been found to be an adequate compromise between model complexity and accuracy (Dutra et al., 2012; Magnusson et al., 2015).

Land surface models (LSM) specifically target global-scale applications, as they were initially developed to represent the lower atmospheric boundary condition of Global Circulation Models. Land surface modeling has seen remarkable progress in recent years, evolving from simple biophysical parametrizations to complex frameworks that incorporate key processes such as soil moisture dynamics, land surface heterogeneity, and plant and soil carbon cycling (Fisher and Koven, 2020; Lawrence et al., 2019). Today's LSMs are thus principally suitable for, and even intended to, study process interactions and feedbacks within the Earth's systems (e.g., Lawrence et al. (2019). However, large challenges in land surface modeling today remain due to uncertainties in process representation, unresolved sub-grid heterogeneity, and the projection of spatial and temporal dynamics of model parameters (Beven and Cloke, 2012; Fisher and Koven, 2020; Fisher et al., 2019; Blyth et al., 2021). It is these limitations that make it difficult to reconcile site-scale experimental data and LSM simulations, hampering their evaluation

and further development. Multi-resolution modelling setups (including the point/site scale) overcome this very limitation (e.g. (Singh et al., 2015; Meissner et al., 2009)), as they allow evaluating a spatially distributed LSM simulation over a large spatial extent, while at the same time certain aspects of the model (i.e. snow depth / snow cover duration) can be validated at the point scale using in-situ observations. This is especially of value if meteorological forcing data (e.g. station data) and/or land-use information as well as model evaluation data is available for a specific point-location.

Today, a strong push is evident towards higher resolution modeling, such as 1km simulations (Schär et al., 2020). While achieving this level of resolution globally over extended periods remains a challenge due to computational limitations, higher resolution allows for a more precise representation of land surface heterogeneity, which directly influences the representation of various key parameters and their associated processes (e.g., Ma and Wang (2022); Rimal et al. (2019); Zhang et al. (2017)). Because depth, duration and variability of seasonal snow cover is strongly affected by topography and thus highly variable in space (e.g., Clark et al. (2011)), higher resolution enables a more detailed characterization of snow distribution, depth, and duration, capturing the spatial variability of snow cover across diverse landscapes (Lei et al., 2022; Magnusson et al., 2019; Essery, 2003). Improved representation of snow cover dynamics has the potential to enhance simulation of surface albedo, which affects the amount of solar radiation reflected back into the atmosphere, and thus influences the overall simulated surface energy balance (Thackeray and Fletcher, 2016; Flanner et al., 2011). An improved representation of snow melt-out date can further directly affect simulation of land surface phenology (Xie et al., 2020).

In this study, we explore how model resolution, and the quality of meteorological and land surface datasets affect the representation of seasonal snow cover dynamics in the Community Land Model 5 (CLM5), a state-of-the-art LSM. More specifically and based on the ideas highlighted above, we hypothesize that with increasing spatial resolution and quality of meteorological and land surface input datasets, the representation of snow cover dynamics and its associated variables in CLM5 can achieve an accuracy comparable to that of a dedicated snow model.

To test this hypothesis, we implement a multi-resolution modelling framework using CLM5. This framework bridges the gap between point/site-scale and spatially distributed land surface modeling, thus allowing us to compare model accuracy across a hierarchy of spatial scales and using diverse evaluation data, while preserving model architecture. This way, confounding effects due to differences in process parametrizations are eliminated, isolating and clarifying the effects of model resolution and input-data, and allowing us to assess the importance of an accurate representation of sub-grid variability within coarser resolution models.

We apply our framework to the spatial extent of Switzerland, including relevant watersheds of neighboring countries. This region provides an ideal setting due to its diverse topography, encompassing both the Swiss Alps and the Swiss plateau. Through a set of modelling experiments, we assess the relative impact of detailed meteorological and land cover information on snow simulations with CLM5 across topographically complex landscapes. Our findings can inform the optimal design of further offline applications of LSMs, for instance 1) to extrapolate local-scale experimental findings; 2) to address the limitations of global-scale, coarse resolution simulations; and 3) to support the interpretation of snow cover information contained in Earth System simulations.

2 Methodology

2.1 Land surface modelling

To investigate the effects of spatial resolution and input datasets in LSMs, we use the land component of the Community Earth System Model (CLM5), an open-source, state-of-the-art, and widely used LSM that simulates carbon, nitrogen, water and energy exchange between the atmosphere and the land surface (Lawrence et al., 2019, 2018). It offers two operational modes: prognostic biogeochemistry (BGC) mode and prescribed satellite phenology (SP) mode. For this study, we focused on running CLM5 in SP mode, where remote sensing-based datasets are used to prescribe spatial extents of Plant Functional Types (PFTs) and Crop Functional Types as well as the PFT-specific monthly Plant Area Index (PAI, sum of Leaf Area Index and Stem Area Index), hence reducing the degrees of freedom compared to prognostic calculations. See Section 2.3.2 for more information.

It's important to note that in SP mode, carbon-nitrogen cycling is not considered, and certain processes such as leaf nutrient limitation and respiration terms are omitted. GPP for the context of this study was approximated by photosynthetic activity, with photosynthesis being limited by carboxylation, light, and export limitations for different plant functional types (Thornton and Zimmermann, 2007; Farquhar et al., 1980). The photosynthesis module in CLM5 is described in detail by Thornton and Zimmermann (2007), Bonan et al. (2011), and Oleson et al. (2010). Simulations were performed with the Leaf Use of Nitrogen for Assimilation (LUNA) routine turned on (Ali et al., 2016). Evapotranspiration in CLM5 is calculated as the sum of transpiration, evaporation (considering soil/snow evaporation, ice/snow sublimation as well as dew), and canopy evaporation following Lawrence et al. (2007).

Spatial resolution influences the representation of spatial heterogeneity in CLM5 which is represented by a sub-grid hierarchical system. Each grid cell is split into different land units (vegetation, glacier, lake, urban, crop). On the second sub-grid level (column-level), potential variability in the soil and snow state variables within the same land-unit is accounted for. However, the vegetation and lake land unit only allow for a single column. Each vegetated column can be further divided up into up to 15 Plant Functional Types (PFTs) or bare ground (this is the third sub-grid level in CLM5, often referred to as the patch-level). Vegetation structure for each PFT is described by monthly varying Leaf Area Index (LAI) and Stem Area Index (SAI), as well as canopy top and bottom heights. All of these values are prescribed in our model setup (satellite phenology mode).

Here, we applied CLM5 both to the regional scale, and to the point-scale, for which CLM5 features a dedicated point mode (PTCLM). It is worth noting that what we refer to as point-scale simulations incorporates fractional state variables (e.g., fractional snow-cover), as the gridded modeling algorithms (i.e., exactly the same as used for large-scale gridded simulations) are directly applied to a single point. From a snow-cover modeling perspective such an approach would be referred to as site-scale, but in order to be consistent with LSM conventions we refer to them as point-scale simulations. As there is no lateral exchange in our model setup (river routing is off), there is no difference in running a dedicated point-simulation and taking out individual grid cells from a regional simulation, apart from the fact that we have additional information at these station locations (e.g. meteorological station data for forcing, exact GPS location for downscaling temperature). We elaborate on our experiments setup for point-scale and gridded simulations in Section 2.2.

2.1.1 Snow and fractional snow cover schemes in CLM5

125 Snow cover provides a convenient means of observing and validating the internal energy turnover of LSMs, and it is the duration of snow cover that influences vegetation periods, ecophysiological processes, and carbon cycles. The snow scheme in CLM5 classifies as a multi-layer snow model with detailed internal-snow-process schemes (Boone and Etchevers, 2001). General snow parametrizations are based on Anderson (1976), Jordan (1991), and Dai and Zeng (1997), with fractional snow cover calculations being based on the method of Swenson and Lawrence (2012). In recent years there have been several updates to the

130 snow-related parametrizations, most notably an inclusion of wind and temperature effects on fresh snow density and an increase in maximum snow layers from 5 to 12 (Lawrence et al., 2019). A detailed description of snow related calculations in CLM5 can be found in Lawrence et al. (2018), but for convenience we also give a brief summary of snow related parametrizations used in CLM5 here. In CLM5, a snowpack can be made up of up to 12 layers, with the lowest being at the snow/soil interface and the uppermost at the snow/atmosphere interface. Each layer is described by mass of water, mass of ice, layer thickness and

135 temperature. Any snowpack smaller than 10cm is treated as a single layer and only described by mass of snow.

Upon falling of solid precipitation on a column, either a new snow layer is initialized (if >10cm) or the snow is added to the present one, whereby combination and subdivision of snow layers is based on Jordan (1991). Mass of ice in each snow layer is calculated based on the rate of solid precipitation reaching the ground, taking into account gains due to frost and losses due to sublimation as well as change in ice due to phase change (melting). Bulk density of newly fallen snow is calculated dependent

140 on air temperature and further increased if wind speeds exceed 0.1 m-1 due to wind compaction, following van Kampenhout et al. (2017). CLM5 includes 4 processes leading to overall snow compaction: (1) destructive metamorphism of new snow (2) snow load (3) melting (4) drifting snow. Mass of water in each layer is dependent on liquid water flow in and out of the layer and change in liquid water due to phase change (melting). For the top snow layer this includes rate of liquid precipitation falling, and evaporation as well as liquid dew. Any water flowing out of the lowest snow layer contributes to surface runoff and

145 infiltration calculations in different CLM5 subroutines.

An essential variable for the energy balance due to its effects on surface albedo is fractional snow-covered area (FSno). FSno is further of importance as CLM5 calculates surface energy fluxes separately for snow-free and snow-covered land unit fractions. FSno in CLM5 is calculated following Swenson and Lawrence (2012), which uses separate parametrizations for the snow accumulation and depletion phase. During accumulation, FSno is calculated as:

150
$$FSno^{n+1} = 1 - ((1 - tanh(0.1 q_{sno} \Delta t))(1 - FSno^n)) \tag{1}$$

where $q_{sno} \Delta t$ quantifies the amount of new snow; $FSno^n$ and $FSno^{n+1}$ denote FSno at the previous and current time step, respectively. During snow-melt, the following parametrization is used:

$$FSno^{n+1} = 1 - [\frac{1}{\pi} acos(2\frac{W}{W_{max}} - 1)]^{n_{melt}} \tag{2}$$

W is the simulated snow water equivalent (SWE) at the current time step and W_{max} is the maximum simulated SWE of

155 the snow season. n_{melt} is the snow covered area shape function, which is determined from σ_{topo}, the standard deviation of

topography within a grid cell by:

$$n_{melt} = \frac{200}{\sigma_{topo}} \tag{3}$$

2.1.2 Rain-snow partioning in CLM5

CLM5 partitions total precipitation into rain and snow according to a linear temperature ramp, resulting in all snow below 0°C,
all rain above 2°C, and a mix of rain and snow for intermediate temperatures. More specfically, the fraction of total precipitation
P falling as rain (q_{rain}) and snow (q_{snow}) at each timestep is calculated as follows:

$$q_{rain} = P(f_p) \tag{4}$$

$$q_{snow} = P(1 - f_p) \tag{5}$$

$$f_p = 0 < 0.5(T_{atm} - T_f) < 1 \tag{6}$$

where T_f is set to 0°C.

2.2 Model experiments with CLM5

Figure 1 provides a general overview of the experimental setup, which includes three aspects. Firstly, we varied the spatial
resolution, ranging from 0.5°(10x6 grid cells) to 0.25°(19x11 grid cells) to 1 km (365x272 grid cells) over the study domain.
As the 0.5°and 0.25°grids were chosen to closely match the extent of the pre-determined 1km grid, grid anchoring might
slightly vary between resolutions. Secondly, we used different meteorological forcing datasets, including a globally available
coarse-resolution dataset (Clim$_{CRU}$), the same global dataset with lapse-rate corrected temperature (Clim$_{CRU*}$), and a high-
resolution regional dataset (Clim$_{OSHD}$). Lastly, we considered two options for land-use information: a global dataset (LU$_{Gl}$)
and a high-resolution dataset (LU$_{HR}$). This approach is intended to cover the multiple facets of resolution: on the one hand, the
spatial resolution of the CLM5 simulations themselves; on the other hand, the 'native' resolution, or level of detail, of the input
datasets, with higher resolution implying better quality of the datasets. Different CLM5 configurations were set up to cover the
variations in spatial resolution, meteorological forcing, and land-use information.

At the 1km scale, CLM5 was run with six different configurations, each using different combinations of meteorological
forcing and land-use information. At the 0.5°and 0.25°resolutions, CLM5 was run with three configurations corresponding to
the respective meteorological forcing datasets and using the global land-use dataset. These regional CLM5 simulations across
the spatial extent of Switzerland and adjacent watersheds of neighboring countries, covering an area of 44,050 km^2, were set
up in an identical way as global simulations.

Additionally, point-scale simulations were conducted at 36 snow-monitoring station locations within the model domain. At
the snow monitoring stations, we focus on the impact of meteorological forcing and land-surface input on CLM5 simulations
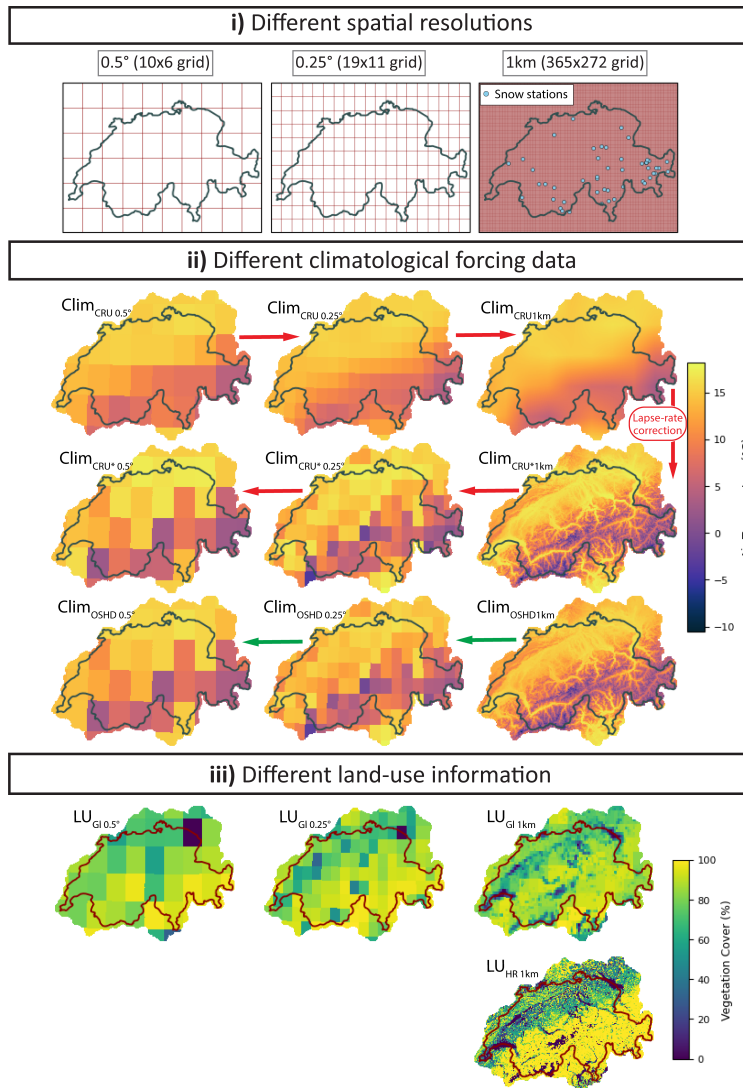
Figure 1. Schematic overview specifying the 3 facets of the experimental setup: Variation of i) spatial resolution, ii) meteorological forcing data and iii) land-use information. i) shows the different grids used, including the locations of the snow stations. ii) shows monthly mean temperature (May 2018) from the different data sources: Globally-available coarse-scale dataset (Clim$_{CRU}$), the same but with a lapse-rate corrected temperature (Clim$_{CRU*}$), and a high-resolution regional dataset (Clim$_{OSHD}$). Note that Clim$_{CRU}$ data is provided at $0.5°$(top left-most panel in ii), and bilinearly regridded to $0.25°$and 1km. Clim$_{CRU1km}$ is then downscaled via a lapse-rate correction to obtain Clim$_{CRU*1km}$, before being up-scaled to $0.25°$and $0.5°$. Apart from temperature, meteorological forcing data is identical for Clim$_{CRU1km}$ and Clim$_{CRU*1km}$ simulations. Clim$_{OSHD}$ data is provided at 1km, and upscaled to $0.25°$and $0.5°$. iii) shows differences in land-use information considered in this study by the example of percentage vegetation cover (sum of vegetation PFTs and crop CFTs).

by first running the same six configurations as for the 1km gridded experiment. While exactly the same modelling framework was used for these point-scale simulations as for the gridded simulations, meteorological forcing was station-specific (e.g. not just the extracted meteorological forcing from the closest 1km gridcell, see 2.3.1 for additional information). Knowing that all 36 snow-monitoring stations are located on non-forested land, we set up 3 additional simulations enabling direct comparison

190 of observations with respective simulations: For each meteorological forcing dataset ($Clim_{CRU}$, $Clim_{CRU*}$, $Clim_{OSHD}$) we set up a simulation where the land-unit was set to be 100% vegetated with PFT 0 (bare ground) rather than using the composite grid-cell from the LU_{HR} and LU_{Gl} dataset, respectively. This additional land use dataset is further refereed to as LU_{nofor}. Model performance evaluation was carried out based on in-situ observations at these stations (see Section 2.4.1 and 2.5.1 for more information).

195 The performance of all gridded CLM5 configurations in simulating seasonal snow cover was assessed against simulations obtained with a dedicated snow model (see Section 2.4.2 and 2.5.2 for more information). Outcomes from the snow cover analyses were complemented by a relative comparison of the different gridded CLM5 configurations for the ecophysiological variables gross primary production and evapotranspiration.

2.3 Input datasets

200 Each CLM5 model configuration requires the following meteorological driving data: incident short and long-wave radiation, air temperature, relative humidity, wind speed, pressure, and precipitation. Additionally, a land surface information file is required.

CLM5 simulations were set-up to run between January 2016 and December 2019, in order to maximize the temporal overlap between the various meteorological forcing datasets and available data for model benchmarking. We further performed 10 years of spin-up by re-cycling through the available input-data. A spin-up was necessary to ensure soil moisture and soil temperature

205 were in approximate equilibrium and not affecting temporal dynamics and physical properties e.g., of the simulated snow cover evolution.

2.3.1 Meteorological Forcing

To assess the impact of meteorological input data quality, we considered three meteorological forcing datasets with increasing level of detail. As an example of a standard global dataset, we used the recent state-of-the-art dataset CRU-JRA (University

210 of East Anglia Climatic Research Unit; of East Anglia Climatic Research Unit; Harris (2019)), which provides near-global (excluding Antarctica) six-hourly meteorological data on a 0.5°latitude x 0.5°longitude grid. CRU-JRA is a merged product of the monthly Climate Research Unit (CRU) gridded climatology (Harris et al., 2014) with the Japanese Reanalysis product (JRA, Kobayashi et al. (2015)). We selected CRU-JRA due to its large timespan (1901-2020), which includes recent years and hence ensures sufficient overlap with our high-resolution forcing dataset (see below), as well as due to its application in

215 the annual Global Carbon Budget assessments (e.g., TRENDY, Friedlingstein et al. (2020)) and in the Land Surface, Snow and Soil Moisture Model Intercomparison Project (LS3MIP, Hurk et al. (2016)). The original 0.5°CRU-JRA dataset was first projected to our model domain using nearest neighbor techniques ($Clim_{CRU0.5°}$), before re-gridding it to 0.25°, 1km and all point locations using bilinear interpolation to obtain $Clim_{CRU0.25°}$, $Clim_{CRU1km}$ as well as $Clim_{CRU^{pt}}$.

As a dataset representing an intermediate level of detail, we upgraded the $Clim_{CRU1km}$ as well as $Clim_{CRU^{pt}}$ datasets by down-
220 scaling temperature data using a temperature lapse rate of -6.5K/1000m, which resulted in the $Clim_{CRU*}$ and the $Clim_{CRU*^{pt}}$
datasets. This approach was intended to account for variations of air temperature within the complex topography of the Swiss
Alps and subsequent refinement of the partitioning of precipitation into snow and rain. We use a global DEM at 0.5° to first
bring temperature to sea-level temperatures by applying negative lapse rates, before using a high-resolution DEM of Switzer-
land to re-lapse temperature (see Figure C1 in the Appendix for both DEMs). For the snow station locations we used the actual
225 GPS measurement of each station, resulting in $Clim_{CRU*^{pt}}$. The updated 1km fields were upscaled back to 0.25° and 0.5° to in-
herit this correction also to the coarser-resolution simulations. This resulted in the $Clim_{CRU*}$ dataset. All other forcing variables
were left identical for $Clim_{CRU1km}$ and $Clim_{CRU*1km}$, as well as $Clim_{CRU^{pt}}$ and $Clim_{CRU*^{pt}}$ simulations.

As input datasets with the highest level of detail, we used meteorological forcing generated according to methods developed
by the Operational Snow Hydrological Service (OSHD), at 1km spatial and 1hour temporal resolution as well as all point
230 locations at 1 hour temporal resolution. Necessary meteorological input variables were all provided by MeteoSwiss (COSMO1
and COSMOE product), and specific downscaling routines were applied e.g., to incoming solar radiation and wind velocity
to optimally capture the influence of complex topography. Of particular relevance to this study is the correction of snowfall
input fields by assimilation of station data according to Magnusson et al. (2014). In the context of this study, this dataset can be
considered a meteorological input specifically optimized for accurate gridded snow cover simulations. The 1km forcing data
235 was then upscaled to the desired target resolution (0.25° and 0.5°) with no smoothing applied. We refer to Mott et al. (2023) for
further details with regards to the $Clim_{OSHD}$ product. The OSHD downscaling algorithms were also applied for each specific
snow station location, resulting in the $Clim_{OSHD^{pt}}$ dataset for the point-scale simulations.

2.3.2 Land-use information

Global-scale land-use information: Input datasets for the land surface are based on the global-scale input dataset commonly
240 used in CLM5, where extents of each land unit and percent plant functional type for each grid cell are derived from MODIS
satellite data (Lawrence and Chase, 2007), as are monthly LAI and SAI values. In a first step, which was performed sepa-
rately for each target resolution (including all point-locations), we used the standard CLM tools (including the Earth System
Modelling Framework (ESMF) regridding tools), to obtain our "global info" land surface dataset (LU_{Gl}, see Figure 1). This
represents a land surface dataset equivalent to that which would be used in a typical large scale LSM/General Circulation
245 Model application. Note that the resolution of the underlying global datasets varied (0.05° for urban/lake/glacier, 0.25° for
vegetated/PFT fractions/LAI and SAI), since we used the most commonly applied CLM5 datasets. This step resulted in the
$LU_{Gl0.5°}$, $LU_{Gl0.25°}$ as well as the LU_{Gl1km} datasets (see Figure 1). In Appendix B we show obtained land unit distributions per
grid cell for all 3 target resolutions (Figure B2, Figure B3 and Figure B4 for LU_{Gl1km}, $LU_{Gl0.25°}$ and $LU_{Gl0.5°}$, respectively),
patch-level PFT distributions (Figures B6, B7, B8) and monthly PAI for temperate needle leaf evergreen trees (Figures B10,
250 B11, B12) as well as boreal broad-leaf deciduous trees (Figures B14, B15, B16).

High resolution land-use information: To obtain an alternative land-use input dataset (LU_{HR1km}) with a higher level of
detail and based on a more up-to-date land use dataset, the LU_{Gl1km} dataset was updated based on a combination of high-

resolution data sources: (1) Copernicus Global Land Service PROBA-V data (2) Copernicus Sentinel-3/OLCI data, and (3) high-resolution national forest mixing ratios derived specifically for Switzerland (100m resolution, Swiss-Federal-Statistical-Office (2013)). In a first step, land unit distributions per grid cell (first sub-grid level in CLM5) were computed using the Copernicus PROBA-V 100m 2019 landcover datasets, which have been shown to be of high spatiotemporal quality (e.g. 79.9% accuracy over Europe for the Discrete Classification dataset, (Tsendbazar et al., 2021)). The native 100m fractional cover datasets were reprojected and regridded to our domain using ESMF tools (with a bilinear interpolation algorithm). We used the Copernicus Builtup-Cover Fraction to obtain the spatial extent of the urban landunit (assumed to be all at medium density), the Crops-Cover Fraction for the crop landunit (assumed to all be rainfed, non-irrigated land), and the level 1 Discrete Classification dataset for lake and glacier land units. The vegetated landunit was derived by adding Copernicus PROBA-V Grass-Cover Fraction, Tree-Cover Fraction, Shrub-Cover Fraction as well as Bare-Cover Fraction together. Minor adjustments were necessary due to regridding artifacts to ensure (a) no pixel exceeded 100% (e.g. around edges of lakes) and (b) each pixel added up exactly to 100% (any non-classified pixels were classified as non-vegetated). Figure B1 in Appendix B shows extents of the LU_{HR1km} dataset for each CLM5 land unit.

For the third sub-grid level (patch-level) of the vegetated landunit, we merged the 100m Copernicus Forest Type layer as well as the 100m Copernicus shrub- and grass cover fraction with Swiss national 100m forest mixing ratio data. The Copernicus Forest Type layer distinguishes between 6 forest classes (needle leaf and broad leaf evergreen forests; needle leaf and broad leaf deciduous forests; mixed forests and unclassified) which were translated to CLM5 PFTs in the following manner: Evergreen trees (both deciduous and broad-leaf) were classified as needle leaf evergreen temperate trees (PFT2), deciduous needle-leaf trees were classified as needle leaf deciduous boreal trees (PFT4) and deciduous broad-leaf trees were classified as broad-leaf deciduous temperate trees (PFT8). All shrubs from Copernicus shrub cover were assumed to be broad-leaf deciduous shrubs (PFT12), and all grass as well as sparsely vegetated cells were classified as C_3 grass. Mixed and unknown pixels were then updated based on the Swiss-wide dataset. If the Swiss-dataset classified it as needle leaf forest, it was set to PFT2, if it was a deciduous forest it was PFT 8, needle-mix and deciduous-mix forest were set to PFT 4 and no wood was classified as C_3 grass (PFT 13). Figure B5 in Appendix B shows percentage PFT fractions of the LU_{HR1km} dataset.

In order to obtain an updated LAI dataset, Copernicus Sentinel-3/OLCI/PROBA-V data at 333m spatial resolution was used, which has a temporal resolution of 3 timesteps per month. We used data for the year 2020, and averaged the 3 monthly timesteps to obtain one layer of LAI data per month. For evergreen PFTs August LAI was used year round, whereas for deciduous PFTs the respective monthly values were used. LAI of pixels where satellite data was not available (snow, clouds) was set to 1. LAIs of crops, shrubs and grasses remained unchanged in the LU_{HR1km} dataset. Figure B9 and B13 in Appendix B show monthly PAI for temperate needle leaf evergreen trees (PFT2) and boreal broad-leaf deciduous tree (PFT 4).

2.4 Test datasets

We used two datasets to assess model performance. The first, consisting of daily snow depth observations from 36 snow stations, allowed to evaluate the performance of CLM5 point-scale configurations in simulating seasonal snow cover against

ground truth data. For an evaluation of the gridded CLM5 simulations, we employed the Flexible Snow Model (FSM2) as a reference snow model for validation.

2.4.1 Snow stations

The 36 snow stations considered cover an elevational gradient, are spread throughout Switzerland (see Figure 1)) and were selected from an exceptionally dense and accurate network of snow observations. Table A1 in the Appendix specifies locations and characteristics of each of these sites. Observations at the station locations consist of daily monitored snow depth (HS), which are collected as part of the snow monitoring networks of either the WSL Institute for Snow and Avalanche Research (SLF) or the Federal Office for Meteorology and Climatology (MeteoSwiss). HS measurements were extracted at a daily timestep and cleaned from obvious outliers (assessed against neighboring stations at similar elevations), which can occur e.g. due to measurement errors (see Mott et al. (2023) for more details).

2.4.2 Snow cover simulations with FSM2

The Flexible Snow Model (FSM2, Mazzotti et al. (2020)), a recent upgrade of the Factorial Snow Model (FSM, Essery (2015)), is an open-source, physics-based snow model of intermediate complexity. Simulations at 250m resolution and point simulations at snow station locations have been specifically set up and calibrated by SLF to run over the extent of Switzerland for the purpose of operational snow water resources monitoring (Griessinger et al., 2019; Mott et al., 2023). At the 250m resolution, model grid cells are subdivided into forest, open, and glacier fractions, with forest cover descriptors derived from a 1m-resolution, LiDAR-based canopy height model available for Switzerland (Mott et al., 2023; Waser et al., 2017). In the absence of high-quality, spatially distributed snow depth observations over the entire extent of Switzerland, these FSM2 simulations were served as ground truth for this study. For comparison with CLM5 output, 250m resolution FSM2 output results were upscaled to 1km without smoothing (e.g. conservative regridding).

2.5 Evaluation of model experiments

2.5.1 Comparing point-scale CLM5 model simulations to station observations of snow depth

Observations at the snow monitoring stations (Figure 1 and Table A1) provide an exceptional opportunity to allow proper assessment of regional model performance. Sub-sampled from a dense, high-quality network of snow observations, these measurements of snow height were used to assess the ability of each station-specific point-scale CLM5 configuration to simulate seasonal snowpack in Switzerland, and were additionally compared to FSM2 simulations. The evaluation of FSM2 runs allowed to assess whether FSM2 is a suitable model to be used as a reference for the gridded simulations.

The stations were binned into three elevational bands (<1000 m.a.s.l, 1000 – 2000 m.a.s.l, >2000 m.a.s.l) resulting in 10, 12 and 14 stations for the low, mid- and high elevation band, respectively. For each station location, the various CLM5 point-scale simulations ($Clim_{CRU1km}+LU_{Gl/HR\ 1km}$, $Clim_{CRU*1km}+LU_{Gl/HR\ 1km}$, $Clim_{OSHD1km}+LU_{Gl/HR\ 1km}$) as well as the FSM2 simulation were compared to observations of snow depth (HS), by computing relative and absolute differences as well as Root Mean

Square Errors (RMSE) and Mean Absolute Errors (MAE) for the time frame between October and July across all 4 simulated snow seasons.

Additionally we use wiggle plots to show the seasonal evolution of model errors for all the point-scale simulations across the 2017/18 season.

2.5.2 Comparing gridded CLM5 model simulations to FSM2 simulations of snow depth

Given that the point-scale evaluation against station data offers an incomplete picture of CLM5 performance in its 'typical' setting (coarse-resolution, gridded) as it is limited to point locations with a narrow range of topographic and vegetation characteristic, we provide a complementary evaluation of all gridded CLM5 simulations against FSM2. This model evaluation was performed at 0.25°resolution, which is a fair target given the complexity of the topography across our modelling domain and its relatively small size, and considering today's ever-increasing computational resources. FSM2 as well as 1km CLM5 simulation results were hence upscaled to 0.25°using a conservative upscaling approach which preserves areal averages. For this purpose, we had to decrease our evaluation domain slightly, as we performed the 1km simulations with a mask running exactly along the edges of our modelling domain, making it impossible to upscale these areas to 0.25°without crude assumptions. The 0.5°simulations were downscaled to 0.25°, and all simulations were evaluated across the same domain.

For the evaluation and quantification of snow-related CLM5 model experiment's performance we used a Taylor diagram (Taylor, 2001), with FSM2 simulations of snow depth at 0.25°as our reference. A Taylor diagram combines centered RMSE, correlation coefficients as well as the spatial/temporal standard deviation and hence describes overestimation or underestimation of the models relative to a benchmark.

Additionally, in order to better understand patterns in model discrepancy as they relate to topography and land cover, we compared simulated snow depth (HS) as a function of elevation for three dates during the 2018/19 winter season (early winter 1-Dec; mid winter 1-Feb; late winter 1-Apr). This comparison was performed at 1km, and only included the six 1km CLM5 simulations as well as FSM2, hence no up-/down-sampling was necessary and the effect of elevation could be assessed over a larger distribution. We further compared changes in land-use information and simulated snow-cover for non-forested vs. forest-dominated grid-cells, allowing an assessment of whether the sensitivity to the chosen dataset depends on the land cover type.

3 Results

3.1 Evaluation of snow simulations at point locations

We begin by focusing on simulated snow depth at point locations. We observed distinct differences in performance using different meteorological forcing datasets in our CLM5 experiments (see Figure 2). The point-scale CLM5 model using global meteorological forcing data (Clim$_{CRU^{pt}}$+LU$_{Gl/HR/nofor}$) showed poor performance in modeling seasonal snow development across all snow station locations. RMSEs were close to 1m for mid-elevation stations and only marginally better for high- and
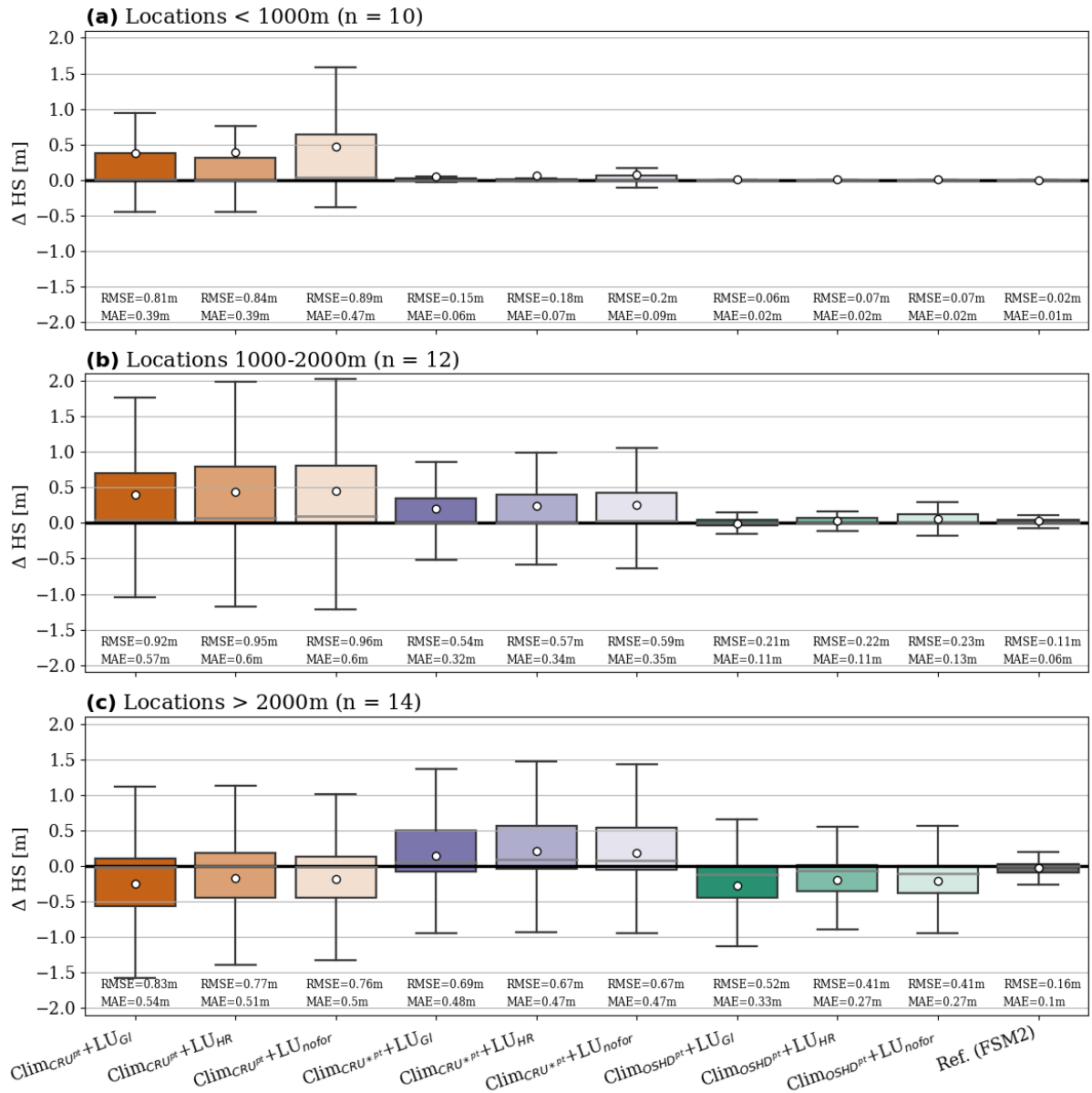
Figure 2. Comparisons of point-scale model simulations to observations of snow depth (HS) across all simulated snow seasons (October-July) for combined (a) low elevation, (b) mid-elevation and (c) high elevation snow station locations. Negative values depict under-estimations of the simulations. Means are shown by the white dots.

low-elevation stations. This demonstrates that these runs fail to accurately represent elevational gradients in temperature and snow amounts, making the error dependent on how closely the characteristics of the station happen to match the characteristics

350 of the coarse resolution grid-cells of the $Clim_{CRU}$ forcing dataset.
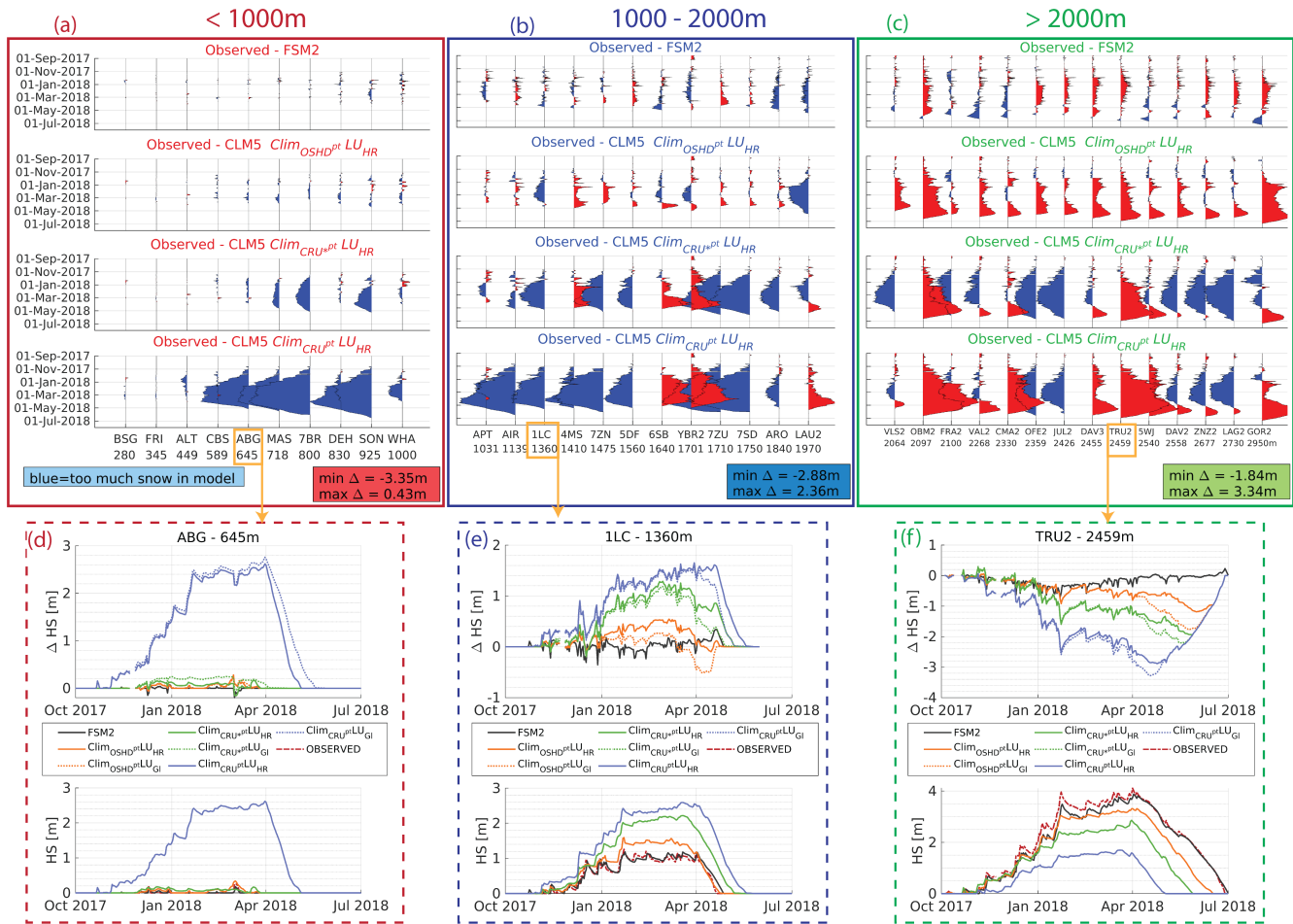
Figure 3. Wiggle plots comparing point-scale model simulations to observations of snow depth (HS) throughout the 2017/18 season for low elevation (a), mid-elevation (b) and high elevation (c) point locations whereby blue denotes too much and red too little snow in the models when compared to observations. (d-f): Absolute difference to observations and seasonal snow depth development for 3 example point locations.

When the lapse-rate based downscaled temperature input was used ($Clim_{CRU*pt}+LU_{Gl/HR/nofor}$) instead, the model's performance improved significantly, particularly at low elevations. At mid- and high elevations the positive impact of a better temperature representation is masked by the overestimated precipitation input when compared to the OSHD dataset (see Figure C2 and Figure C4 in the Appendix for a comparision of precipitation forcing between the CRU and the OSHD forcing

355   dataset). The overestimation of snow at mid- and high elevations of the $Clim_{CRU*}$ dataset is hence a direct result of overestimated precipitation along the Alps.

The CLM5 model forced with OSHD data ($Clim_{OSHD pt}+LU_{Gl/HR/nofor}$) demonstrated the best performance across all three elevation bands, with only minor errors in low- and mid-elevation locations (e.g., RMSE/MAE of 0.22/0.11m for mid-elevation

Clim$_{OSHD^{pt}}$+LU$_{HR}$ simulations). These simulations overcome the 'too much solid precipitation problem' outlined above as the OSHD precipitation forcing dataset is optimized by data assimilation. The underestimation at high elevations is likely due to snow process representation in the model (combination of too fast settling and too efficient melt, see Figure 3f). Generally, these results indicate that the CLM5 model forced with OSHD data approach the accuracy of a dedicated snow model (FSM2), at least when assessed at point locations.

Figure 3 further illustrates these results, as it features wiggle plots as well as seasonal snow development for selected snow station location throughout the 2017/18 winter season. It is apparent across all elevation bands that FSM2 simulations match observations the closest (discussed in more detail in Section 3.1.1), and that CLM5 forced with OSHD data is the next best. CLM5 with global meteorological forcing data (Clim$_{CRU^{pt}}$) performs poorly with maximal errors of over 3m. These biases are persistent throughout the snow season, whereas snow depth is mostly overestimated below, and underestimated above 2000m, respectively.

Regarding the effects of the land-use information dataset, we observed that the choice of land-use information only had a small impact on simulated snow depth (Figure 2). We include simulations using the global, the high-resolution, as well as the non-forested land use dataset (LU$_{Gl}$, LU$_{HR}$, LU$_{nofor}$ respectively). While a slight improvement was seen when using the high-resolution land-use information dataset (LU$_{HR}$) at high elevations for all three sets of meteorological forcing data (reducing RMSE by -0.06m/-0.02m/-0.11m for Clim$_{CRUpt}$/ Clim$_{CRU^{*}pt}$/ Clim$_{OSHDpt}$ simulations, respectively), no substantial differences or marginal decreases in model performance were observed for the lower two elevation bands. This is further underlined by Figure 3d-f. Simulating open, non-forested sites (LU$_{nofor}$) only had marginal effects on model performance: For low and mid-elevations a slight decrease in model performance is apparent for all three meteorological forcing datasets, whereas at high elevations differences are virtually non-existent. This can be explained by the larger variety in land-unit distributions at lower elevations, while at high elevations differences between the two datasets remained small. Ultimately, it can be seen that, at coarse model resolution, the effect of meteorological forcing data is substantially larger in comparison to differences arising from the choice of land surface information.

3.1.1 Accuracy of FSM2 point-scale simulations

Across all elevation bands, the FSM2 simulations closely matched the observations, with only minor errors at low and mid elevations during the 2017/18 season (Figure 2). At high elevations, the FSM2 model slightly underestimated snow depths, which can be assessed in more detail in Figure 3. Figure 3 visualizes the superior performance of FSM2 in comparison to all CLM5 model experiments, further justifying using FSM2 model simulations as our ground truth for the gridded simulation comparisons in Section 3.2.

3.2 Evaluation of gridded snow simulations

The comparison of gridded simulations with CLM5 to FSM2 reference simulations allows us to investigate all three facets of this study: Effects of resolution, effects of meteorological forcing data, and effects of land-use information data. To this end, we consider gridded simulations of snow depth from all 12 different CLM5 configurations (see Figure 1(ii) and (iii))
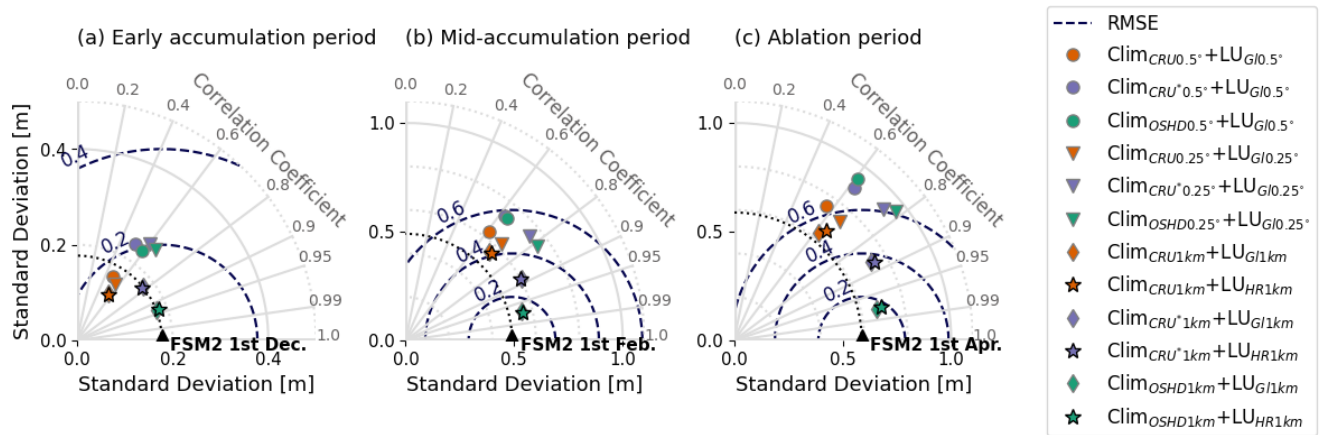
Figure 4. Taylor plots (Taylor, 2001) for comparisons of simulated snow-depth (HS) between all 12 different CLM5 configurations and the reference snow simulation (FSM2, dark grey) during (a) early accumulation season (1-Dec), (b) mid-accumulation period (1-Feb) and (c) ablation period (1-Apr) throughout four winter seasons (2015/16, 2016/17, 2017/18, 2018/19). The plotted statistical metrics allow for evaluation and quantification of CLM5 model experiments performance, based on centered RMSE (directly proportional to the distance away from the reference (=FSM2)), correlation coefficients (azimuthal position) and the spatial/temporal standard deviation (radial position from the origin) which determines overestimation or underestimation of the models.

and compare them to FSM2 simulations (Figure 4). Our analysis is performed across all four snow seasons, and at 0.25°. Additionally we investigate how the accuracy of CLM5 varies as a function of elevation by comparing all 1km simulations against FSM2 (Figure 5) for the 2018/19 season. For both analysis we differentiate between early accumulation period (1st December), mid-accumulation period (1st of February) and ablation period (1st of April).

Increasing the level of detail in meteorological forcing data has the largest effect on accuracy of simulated seasonal snow cover, especially when simulating at 1km. CLM5 runs with OSHD-based input data outperform all CRU- and CRU*-based simulations at all three points in time during winter (e.g., RMSE $Clim_{OSHD1km}+LU_{Gl1km}$: 0.07, 0.14, 0.18m vs. RMSE $Clim_{CRU*1km}+LU_{Gl1km}$: 0.12, 0.29, 0.37m vs. RMSE $Clim_{CRU1km}+LU_{Gl1km}$: 0.15, 0.41, 0.53m for early, mid, and end-winter respectively; Figure 4)) as compared to FSM2 simulations. The postitive effects of lapse-rate corrected temperatures on model performance ($Clim_{CRU1km}$ vs. $Clim_{CRU*1km}$) are pronounced during mid-accumulation and ablation period, where performance is substantially enhanced, while during early accumulation only correlation and standard deviation is improved when moving from $Clim_{CRU1km}$ to $Clim_{CRU*1km}$. The reason behind this is that during early season snow height tends to be small anyways, but once snow amounts become substantial the effect of a lapse-rate correction in the context of partitioning precipitation into rain and snowfall becomes more evident, and simulation results diverge. A simple lapse rate correction that accounts for high-resolution topography hence already brings a lot of benefit relative to a coarse-resolution dataset.

Figure 5 further illustrates these findings: Focusing in on only one representative season (2018/19) and looking at simulated snow-depth as a function of elevation, elevational behaviour of FSM2 is matched closest by CLM5 simulations using OSHD-

based forcing data, with most discrepancies occurring during the ablation period at high elevation. Downscaling temperature has a substantial effect on performance, allowing $Clim_{CRU*1km}$ to closely match performance of $Clim_{OSHD1km}$.

However, the benefits of a higher level of detail in the meteorological forcing are negated when model resolution itself is decreased. Comparing results of CLM5 configurations that differed in resolution only, a large decrease in accuracy is evident for the OSHD- and CRU*-based runs when moving from 1km to 0.25°, while further coarsening to 0.5° only has a marginal effect. This is because the evolution of snow cover is shaped by non-linear process interactions (e.g., temperature fields affect both snowpack energetics and its mass balance by dictating precipitation phase) that are 'lost' when meteorological input is averaged spatially. Our simulations suggest that a model resolution higher than 0.25° is essential to capture the spatial heterogeneity of snow cover evolution processes in the complex terrain present in our study domain. In accordance with this finding, resolution did not have much impact on the performance of the CRU-based runs, since simple regridding without additional consideration of topographic effects on the meteorological drivers does not bring any added values in capturing the non-linear processes shaping snow cover dynamics in complex terrain.

Ultimately, throughout the four modeled years, and averaged over the model domain, substantial differences in simulated snow-cover between the various CLM5 configurations are evident (Figure 4). In a similar manner to the point-scale CLM5 simulations, results revealed considerable improvements in simulated snow cover accuracy when using high-confidence forcing data (Figure 2, Figure 4), with CLM5 in our best-effort scenario ($Clim_{OSHD1km}$+LU_{HR1km} simulation) almost reaching the level of a dedicated snow model also in a gridded application. This becomes especially apparent when looking at the high correlation coefficient of the $Clim_{OSHD1km}$+LU_{HR1km} simulation in Figure 4. However, degraded model performance between the 1km and the 0.25°configurations suggests that in order to actually benefit from the added value of high-quality forcing data, a sufficiently high model resolution remains necessary when applying CLM5 in topographically complex regions.

In order to better understand why the effect of land-use data in our results was minimal, we further investigated the link between changes in land-use information and simulated snow-cover for non-forested vs. forest-dominated grid-cells. Figure 6 compares differences in PAI (averaged across all PFTs, averaged between January-March) across the model domain between LU_{HR1km} and the LU_{Gl1km} with simulated snow height for 1-Feb-2018. We show that the majority of snow-dominated pixels correspond to pixels with little change in PAI between the high-resolution and the global land-use datasets (e.g. non-forested areas). Pixels with large changes in PAI on the contrary tend to be located in the lowlands, with little snow throughout the season. This demonstrates that the impact of land-use data is masked by the many pixels with much snow but little change in PAI. The low sensitivity we find with regards to land-use forcing is hence mostly a symptom of the limited overlap between snow dominated and forested areas in our model domain.

3.3 Simulation of ecophysiological variables

While the previous sections focused on the representation of snow cover, an asset of LSMs relative to dedicated snow models such as FSM2 is that they include a more comprehensive description of land surface processes and state variables, allowing the interaction between these to be investigated. In this final part of our analysis, we thus extend our focus to ecophysiological parameters to showcase effects of spatial resolution, meteorological forcing and land-use information beyond snow cover. In
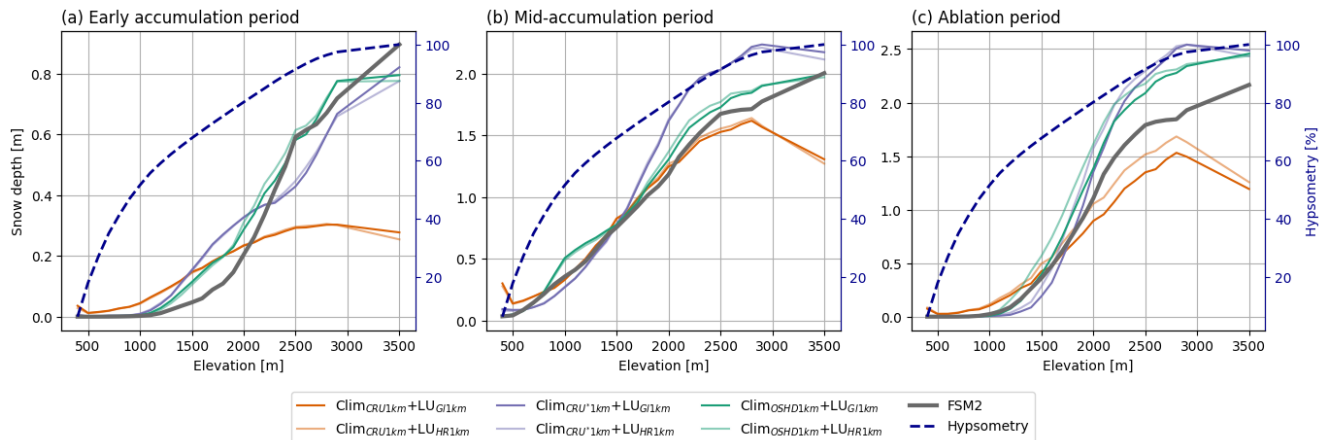
Figure 5. Simulated snow depth (HS) as a function of elevation during (a) early accumulation season (1-Dec), (b) mid-accumulation period (1-Feb) and (c) ablation period (1-Apr) for the 2018/19 winter season. We contrast elevational dependency of FSM2 (dark grey) with all six 1km CLM5 configurations. The dark blue dashed line represents hypsometry across the model domain (Switzerland+).

lack of a reference model for evaluation, we present a relative comparison between spatially distributed (a) simulated mean total GPP for 2016-2019 as well as (b) total ET during 2017 in Figure 7. To single out the impact of each facet of our study, in each plot $Clim_{OSHD1km}+LU_{Gl1km}$ is compared with the $Clim_{OSHD1km}+LU_{HR1km}$ simulation (effect of land-use information), with the $Clim_{CRU1km}+LU_{Gl1km}$ (effect of meteorological forcing) as well as with the $Clim_{OSHD0.5°}+LU_{Gl0.5°}$ simulation (effect of spatial resolution).

For GPP, sensitivity of land-use information outweighed sensitivity of meteorological forcing. Higher level of detail in the land use data caused both increases and decreases in GPP across the model domain, while improved meteorological input had a more systematic effect.

The choice of land surface information datasets, on the other hand, only showed marginal effects on simulated ET, but the effect of meteorological forcing results in substantial differences in simulated ET (up to 26% when averaged over the entire model domain). This effect is especially pronounced along the Swiss Alps, where complex terrain leads to differences in precipitation patterns captured by the two forcings (see Figures C2, C4, C3 in the appendix for comparison of precipitation patterns in the forcing datasets). Temperature differences between the two forcing datasets further contributed to the differences, as it is precisely along the Swiss Alps where $Clim_{CRU1km}$ does not capture topographic effects on temperature.

For both GPP and ET, model resolution in isolation strongly affects the spatial patterns due to non-resolved surface heterogeneity at coarse resolution. Discrepancies between the simulations are less directional and hence difficult to quantify.
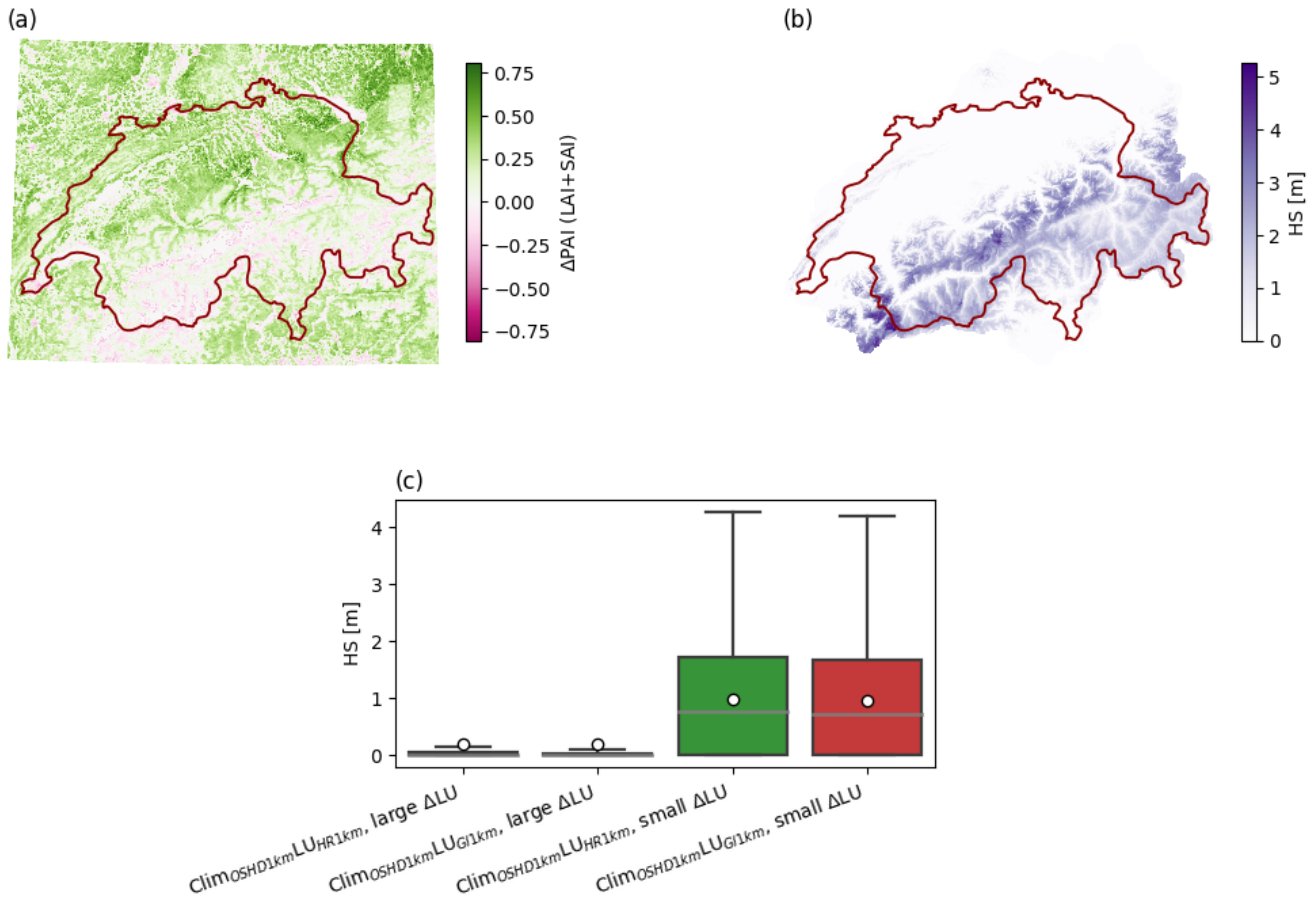
Figure 6. Links between change in land-use and simulated snow cover: (a) PAI difference between the LU_{HR1km} and LU_{Gl1km} dataset, whereby PAI (LAI+SAI) is averaged across all PFTs as well as between January and March. (b) Snow depth on 1-Feb-2018 as simulated by CLM5 $Clim_{OSHD1km}+LU_{HR1km}$. (c) Comparison of snow height distributions on 1-Feb-2018 for $Clim_{OSHD1km}+LU_{HR1km}$ and $Clim_{OSHD1km}+LU_{Gl1km}$, each for pixels with a large change in overall PAI (>0.25) and a small change in overall PAI (<0.25).

4   Discussion

460   This study used CLM5 to offer a multi-scale assessment of the representation of seasonal snow in complex topographic terrain, by evaluating simulated snow depth against a wealth of station data, as well as gridded FSM2 simulations. The multi-resolution setup and a suite of model experiments allowed assessment of several aspects (impact of resolution and input datasets), in spatially and temporally resolved manner, while leveraging diverse reference datasets.

Evaluation against station data showed that CLM5 itself is capable of achieving performance similar to a dedicated snow
465   model when applied in point mode and with the best available input data (land use info and meteorological forcing; $Clim_{OSHD1km}+LU_{HR1km}$). Differences to station data are largest at high elevation, where CLM5 underestimates snow cover. As this bias persists through-
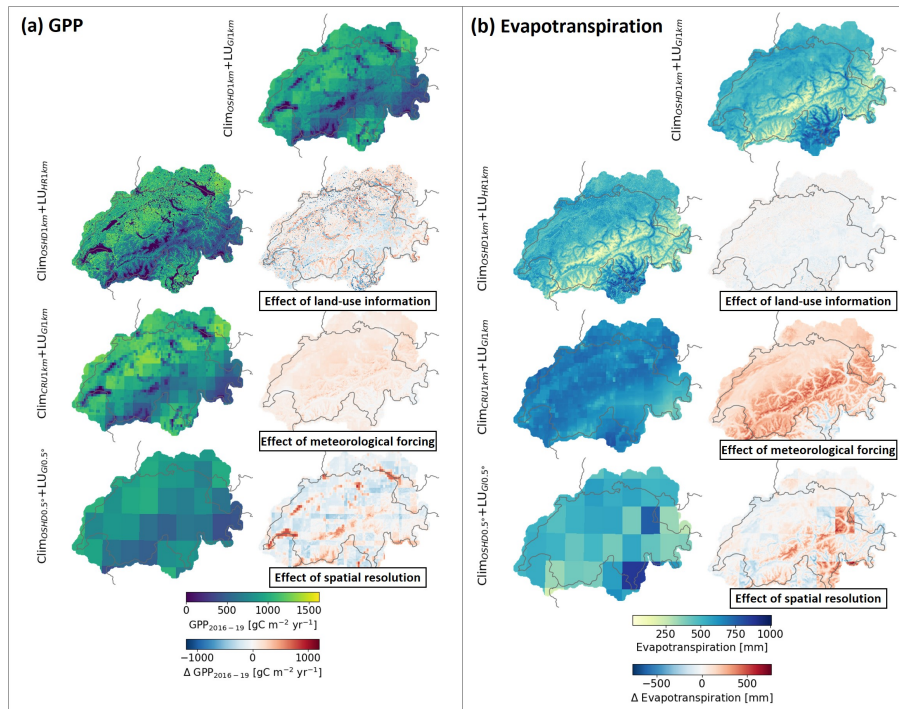
Figure 7. Spatial comparison of CLM5-simulated a) yearly GPP (mean 2016-2019) and b) Evapotranspiration for 4 different CLM5 configurations of this study, showing absolute values as well as relative differences to investigate the effect of land-use information, the effect of climatological forcing and the effect of spatial resolution.

out the season, it is likely due to a combination of accumulation and internal snowpack properties (e.g. the settling parameterization) and melt processes. Tracking down the exact mechanism would require a process-level comparison beyond the scope of this study, but it should be noted that in FSM2 as set up by OSHD parameters such as the effective roughness length and
470   fresh snow albedo vary spatially (e.g. with elevation); future studies could assess whether such spatially variable parameters could benefit CLM5 snow simulations as well.

    Rather than point-mode applications, however, CLM is intended for gridded applications over large areas. This is where our modelling experiments provided interesting insights into the performance of different CLM5 configurations. We found that the most accurate snow cover simulations for Switzerland, with results comparable to those of the operational snow-
475   hydrological model (FSM2), were achieved using high-resolution meteorological forcing data (OSHD) and a 1km resolution that fully resolved landscape heterogeneity. This confirmed our hypothesis, which stated that with increasing spatial resolution and quality of meteorological and land surface input datasets, the representation of snow cover dynamics and its associated variables in CLM5 can achieve an accuracy comparable to that of a dedicated snow model. These findings align with previous studies (e.g., Lüthi et al. (2019)).

Performance of snow-cover simulations is thus constrained by the capability of the meteorological input to capture topographic effects (e.g., improved estimation of precipitation phase due to the high resolution temperature fields) and precipitation patterns, which is a function of both input type (e.g., $Clim_{OSHD}$ vs. $Clim_{CRU}$) and model resolution. Indeed, the fact that aggregating OSHD-based forcing data for coarser resolution simulations drastically reduced simulation accuracy evidenced the need for resolutions higher than 0.25° for snow simulations in topographically complex terrain.

The lapse-rate corrected results ($Clim_{CRU*}$) suggest that in the absence of native high-resolution input data, increasing model resolution through interpolation of input fields with a simple lapse-rate correction of temperature fields can already account for an important topographic effect and thus positively impact model results. This approach, however, cannot provide the high-quality precipitation data achieved with data assimilation based techniques (as used in the OSHD forcing). Model errors are thus inherently linked to uncertainty in precipitation input, which can cause both over and underestimations of snow (in the case of the evaluation at the stations, errors in precipitation (overestimation) overcompensated the underestimation seen in the $Clim_{OSHD}$ simulations for the highest elevation band).

Where model simulations at high resolution are unfeasible (e.g. limited by computational constraints), results from our study suggest that developing a sub-grid parametrization that accounts for the impact of topography on precipitation partitioning as well as on temperature could be a promising approach.

Snow simulations were not sensitive to land-use data, but this is likely due to the distribution of land-units within our model domain, as most snow-dominated grid-cells only saw small changes when moving from the global (LU_{Gl1km}) to the high-resolution land use dataset (LU_{HR1km}). Previous mulit-resolution studies with FSM2 have shown that land-use data does indeed affect simulated snow dynamics (Mazzotti et al., 2021). However, for other ecophysiological variables (GPP in this case) we showed a large effect of land-use data. Today, a plenitude of new detailed land cover datasets are emerging thanks to advances in satellite remote sensing datasets, which should be exploited for land surface modelling.

To gain a more comprehensive understanding, it would be beneficial to repeat such a model experiment in an arctic environment rather than just an alpine one, as high latitudes are critical components of the rapidly changing climate system. Changes in land-use datasets are likely to have a greater effect in such environments, as larger extents of forested areas overlap with seasonally snow-covered areas.

Additionally, it is important to note that all simulations in this work were conducted in satellite phenology mode. Direct assessments of linkages between simulated snow cover and ecophysiological parameters were hence not possible. Future studies should compare CLM5 simulations with prognostic vegetation and biogeochemistry modes turned on to enable a more detailed analysis of the terrestrial carbon and nitrogen cycles, as well as evapotranspiration fluxes.

Uncertainty remains in climate change impact assessments using LSM projections (e.g., Shrestha et al. (2022); Yuan et al. (2021, 2022)), with two major sources of uncertainty being the effects of resolution and the quality of meteorological input data (especially precipitation, Peters-Lidard et al. (2008)) on LSM simulation outputs. Quantifying such uncertainties is imperative to further increase the predictive power of climate impact models. Furthermore, given the complexity of state-of-the art LSMs, an understanding of the ways different parts/modules of LSMs interact with each other is more important than ever, as climate change impacts are not isolated, but highly interconnected processes (Zscheischler et al., 2018; Ridder et al., 2021). It is there-

fore of great importance to investigate how exchanges and interactions between model components are represented, rather than assessing process representation for each model component separately (Blyth et al., 2021), which ultimately requires multi-disciplinary community efforts (Ciscar et al., 2019). Multi-resolution modelling frameworks as used for this study have large potential to help with such endeavors and provide critical insights into ecosystem responses to environmental change. More specifically, it can help identify both the key processes for which high spatial resolution and high-fidelity input data are necessary, as well as quantify the minimum resolution needed to resolve these processes accurately. Such modelling experiments should be prioritized in the future, ideally in combination with experimental manipulations (e.g., increase the availability of nitrogen or carbon dioxide in the system) as suggested by Wieder et al. (2019).

5 Conclusions

Using multi-resolution modeling experiments to quantify and potentially constrain uncertainties in land surface modeling, we highlight the importance of input data quality and spatial resolution in accurately representing seasonal snow cover across scales. We found that CLM5 is capable of achieving performance similar to a dedicated snow model when using high-resolution meteorological forcing data and a 1km resolution that represented landscape heterogeneity well. Results further showed that a simple lapse-rate correction of temperature fields can already account for an important topographic effect on precipitation partitioning and has large positive impacts on model performance. Aggregating high-resolution forcing data for coarser resolution simulations drastically reduced simulation accuracy, further underlining the need for resolutions higher than $0.25°$ for snow simulations in topographically complex terrain. Snow simulations were less sensitive to land-use data compared to meteorological data, but eco-physiological variables (GPP) are strongly affected by the choice of land-use forcing. The results clearly demonstrate the utility of high spatial resolution and regionally detailed forcings in land surface models to better quantify and constrain the uncertainties in the represented processes, with profound implications for climate impact studies. More generally, this study highlights the utility of multi-resolution modeling experiments which bridge the gap between point-scale and spatially distributed land surface modeling.

Code and data availability. All scripts used for simulation setup and analysis can be found at https://github.com/johanna-malle/CLM5_CH. FSM2 snow simulation results can be downloaded from https://www.envidat.ch/dataset/seasonal-snow-data-wy-2016-2022. Upon publication, all CLM5 simulation results presented in this study will be available from the WSL data repository Envidat at their website under https://www.envidat.ch/.

Appendix A: Point-scale CLM5 model simulations at snow stations

Site	Name	Latitude (CH1903)	Longitude (CH1903)	Elevation [m a.s.l.]
BSG	Brissago	108390	698200	280
FRI	Frick	262700	643353	345
ALT	Altdorf	191700	690960	449
CBS	Chaebles	186320	552495	589
ABG	Labergement	178770	527540	645
MAS	Marsens	167220	571440	718
7BR	Brusio	126780	807070	800
DEH	Degersheim	247600	732600	830
SON	Sonogno	134050	703640	925
WHA	Wildhaus	229570	746130	1000
APT	Alpthal	212930	696860	1031
AIR	Airolo	153400	688910	1139
1LC	LaComballaz	136580	572640	1360
4MS	Muenster	148900	663420	1410
7ZN	Zernez	175259	802751	1475
5DF	DavosFluelastr	187400	783800	1560
6SB	SanBernardino	147290	734110	1640
YBR2	Ybrig	210311	705399	1701
7ZU	Zuoz	164590	793350	1710
7SD	Samedan	156400	786210	1750
ARO	Arosa	183320	770730	1840
LAU2	LauenenTruettlisbergpass	141633	595482	1970
VLS2	ValsAlpCalasa	170764	735166	2064
OBM2	OberMeielGrossStand	141183	582760	2097
FRA2	FrascoEfra	132853	708906	2100
VAL2	VallasciaSchneestation	155980	690126	2268
CMA2	CrapMasegnSchneestation	189875	733050	2330
OFE2	OfenpassMurtaroel	168460	818233	2359
JUL2	JulierVairana	149949	773049	2426
DAV3	DavosHanengretji	184616	778292	2455
TRU2	TrubelbodenSchneestation	135519	611306	2459
5WJ	Weissfluhjoch	189230	780845	2540
DAV2	DavosBaerentaelli	174726	782062	2558
ZNZ2	ZernezPuelschezza	175078	797312	2677
LAG2	PizLagrevSchneestation	147050	777150	2730
GOR2	GornergratSchneestation	92900	626700	2950

Table A1. Name, location and elevation of all snow station locations used in this study.

Appendix B: Land-use information data sets
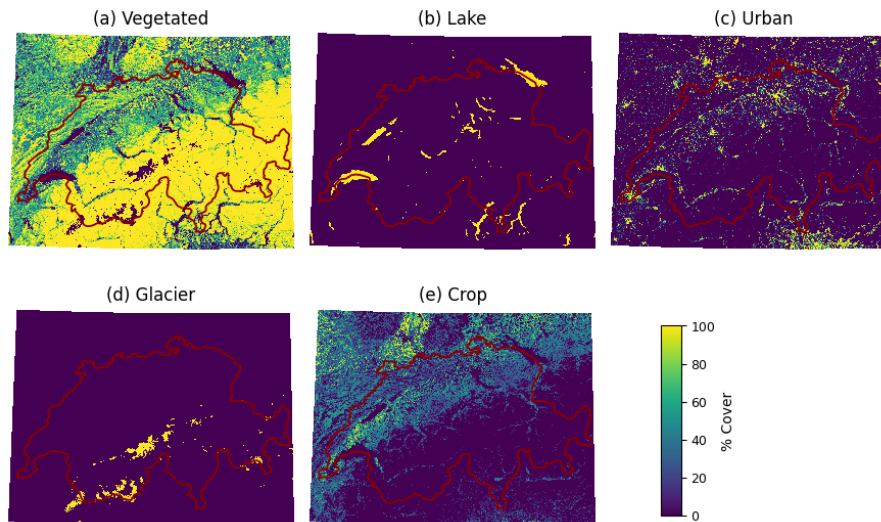
Figure B1. Land unit distribution per grid cell for the high-resolution 1km land use dataset (LU$_{HR1km}$) as used in this study. The 5 CLM5 land units sum up to exactly 100%.
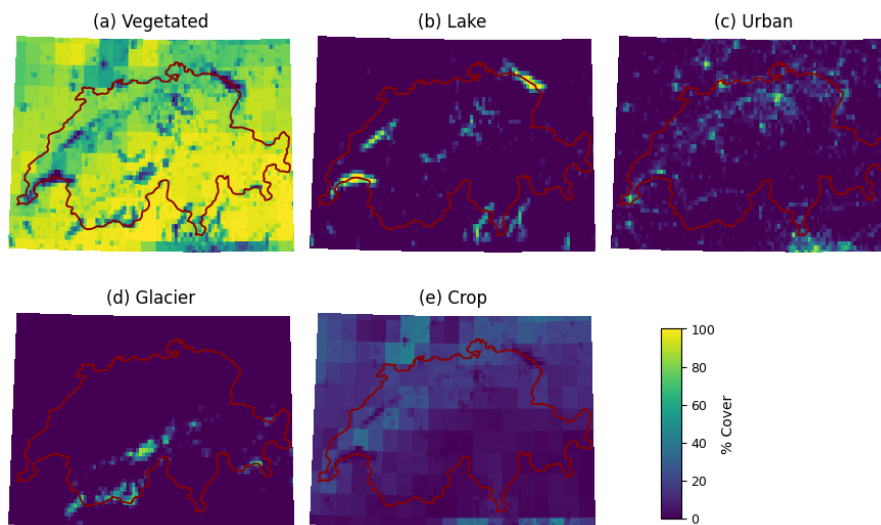
Figure B2. Land unit distribution per grid cell for the global 1km land use dataset (LU$_{Gl1km}$) as used in this study. The 5 CLM5 land units sum up to exactly 100%.
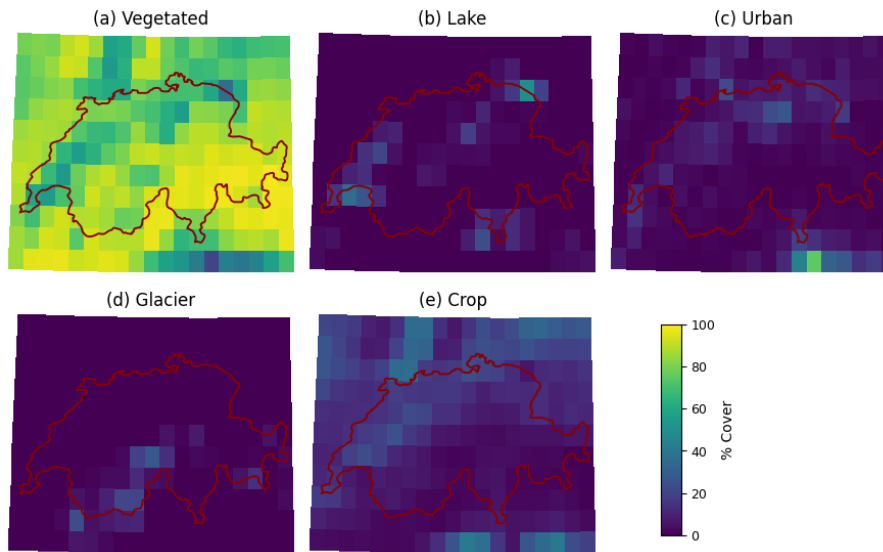
Figure B3. Land unit distribution per grid cell for the global 0.25° land use dataset (LU$_{GI0.25°}$) as used in this study. The 5 CLM5 land units sum up to exactly 100%.
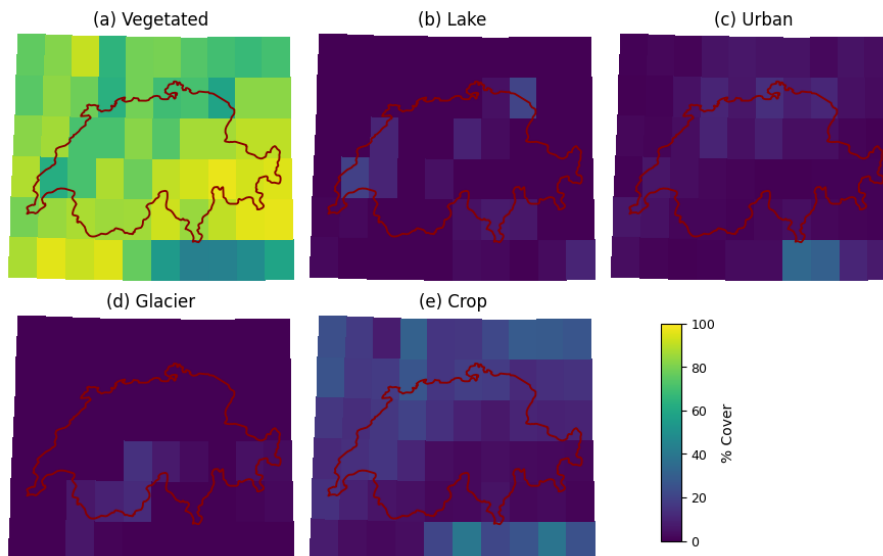
Figure B4. Land unit distribution per grid cell for the global 0.5° land use dataset (LU$_{GI0.5°}$) as used in this study. The 5 CLM5 land units sum up to exactly 100%.
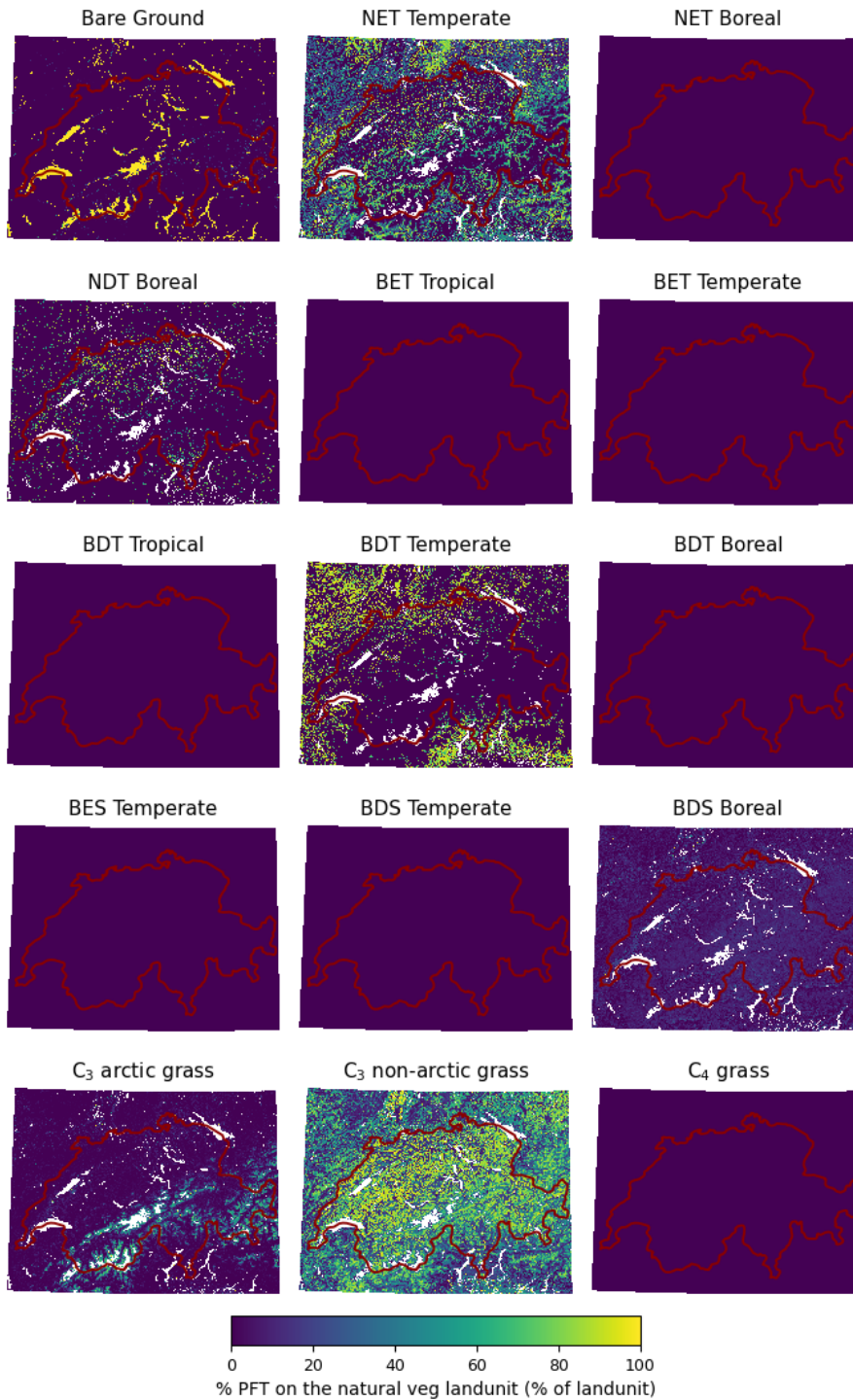
Figure B5. Patch-level Plant Functional Types (PFT) distributions for the high-resolution 1km land use dataset (LU$_{HR1km}$) as used in this study.
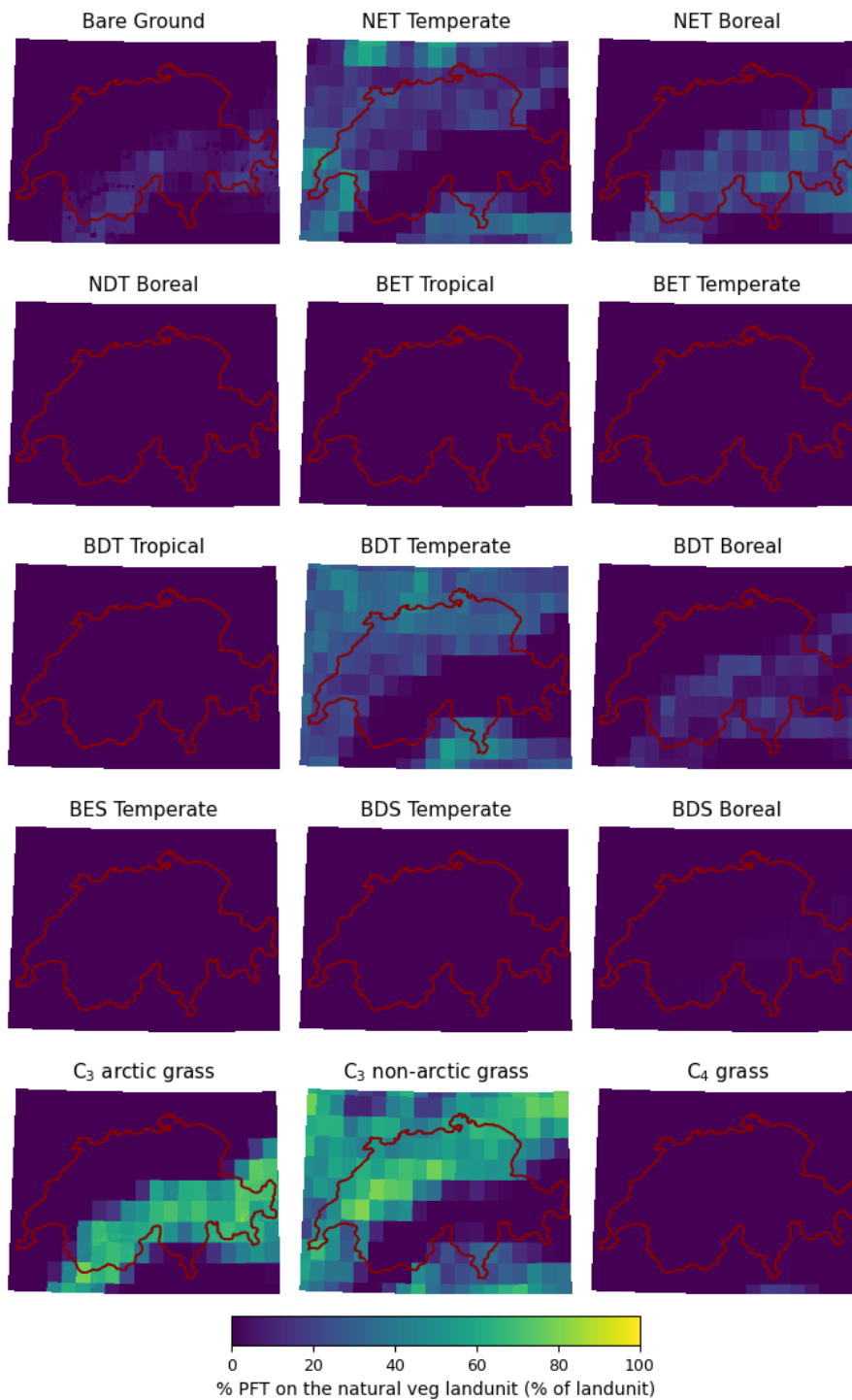
Figure B6. Patch-level Plant Functional Types (PFT) distributions for the global 1km land use dataset (LU$_{Gl1km}$) as used in this study.
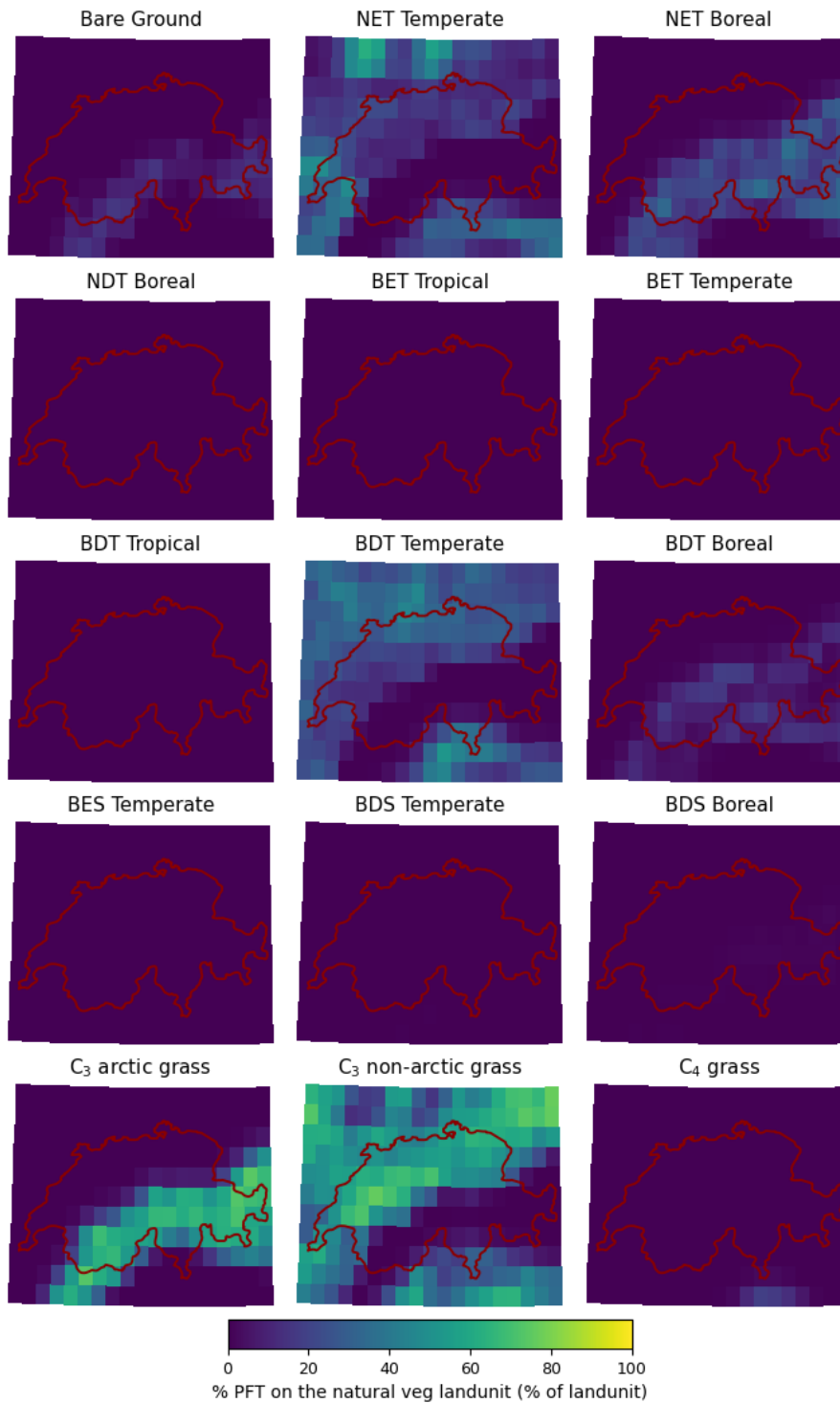
Figure B7. Patch-level Plant Functional Types (PFT) distributions for the global 0.25° land use dataset (LU$_{Gl0.25°}$) as used in this study.
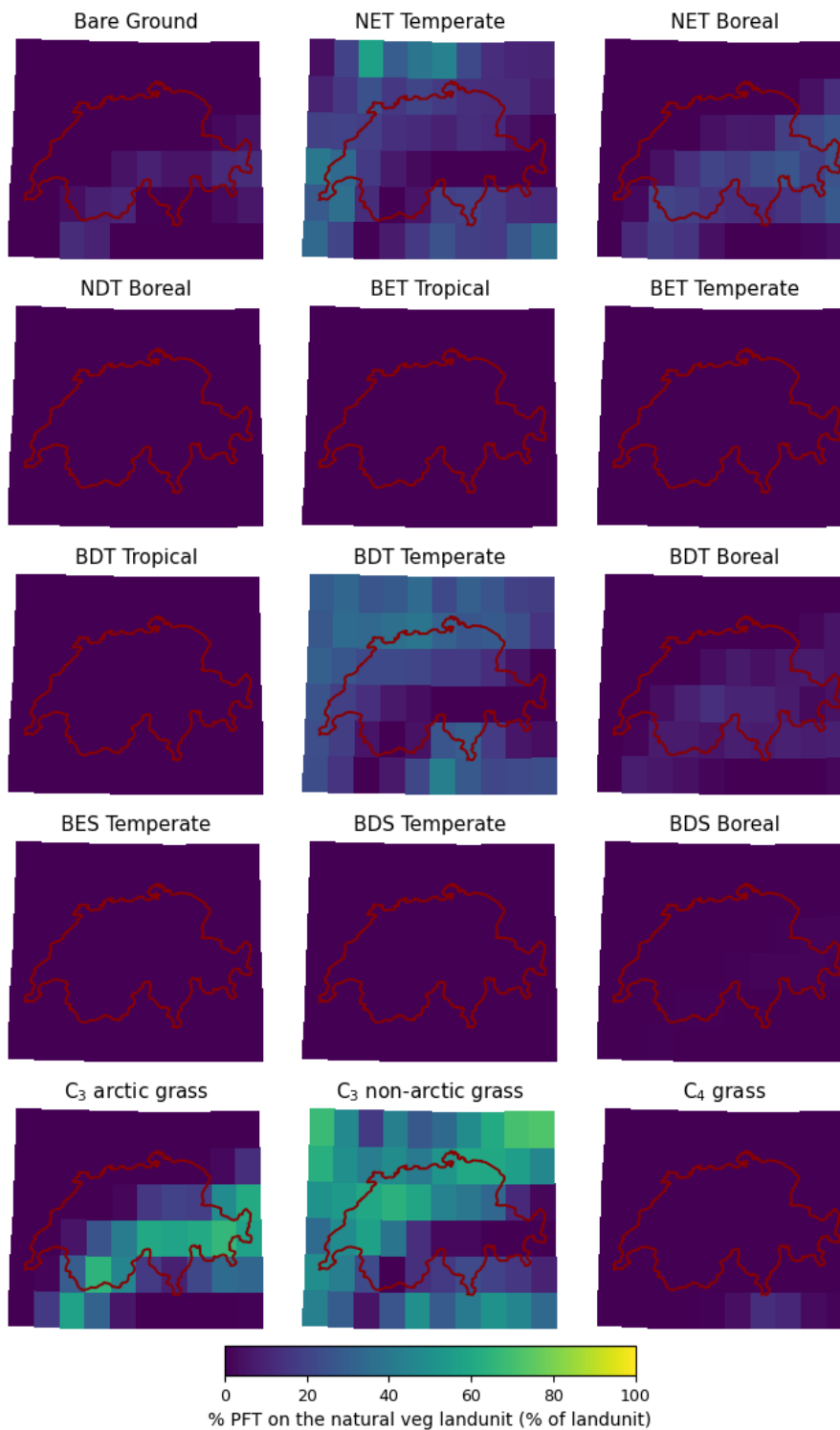
Figure B8. Patch-level Plant Functional Types (PFT) distributions for the global 0.5° land use dataset ($LU_{GI0.5°}$) as used in this study.
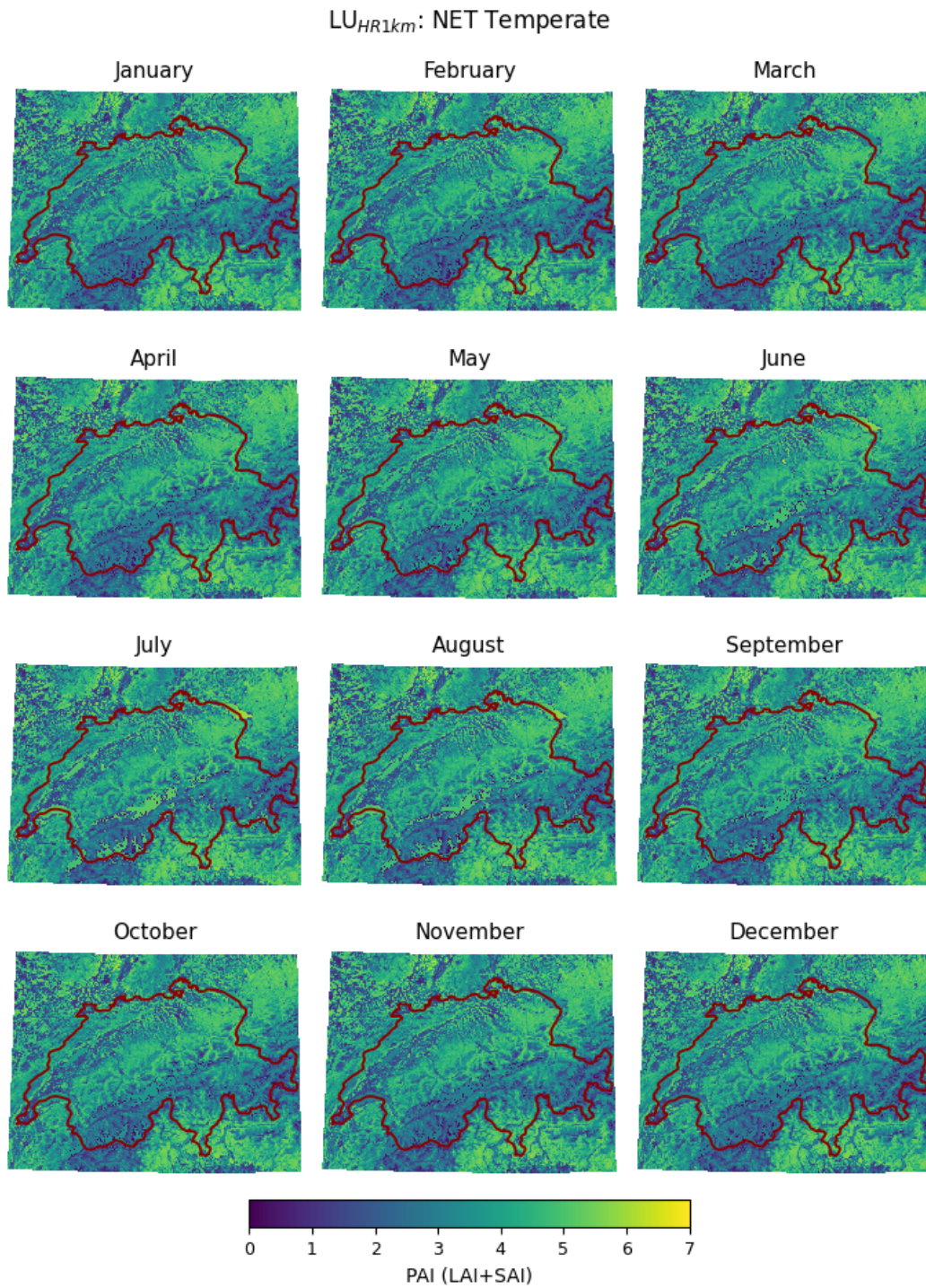
Figure B9. Monthly Plant Area Index (PAI) for temperate needle leaf evergreen trees for the high-resolution 1km land use dataset (LU$_{HR1km}$) as used in this study.
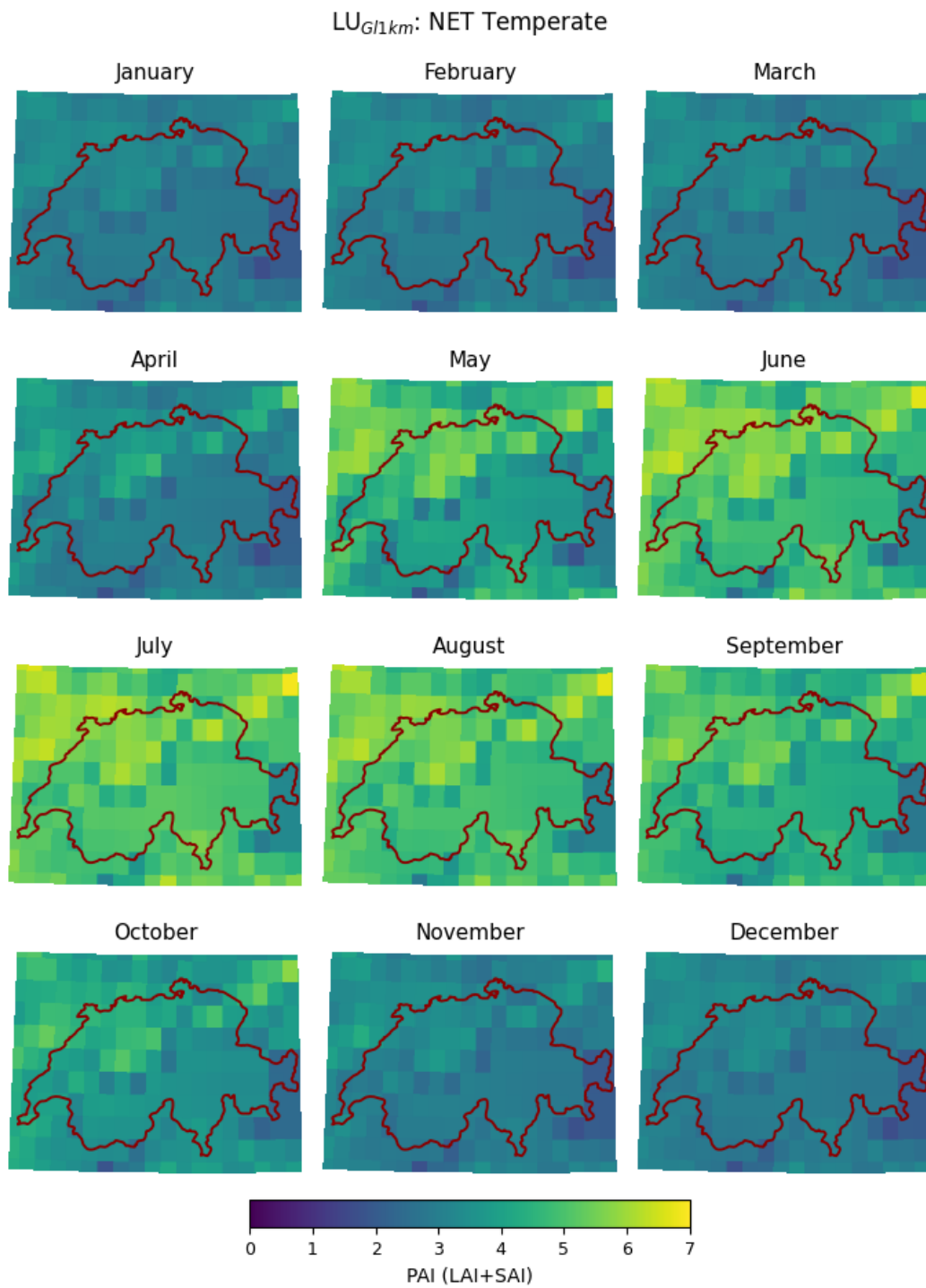
Figure B10. Monthly Plant Area Index (PAI) for temperate needle leaf evergreen trees for the global 1km land use dataset (LU$_{Gl1km}$) as used in this study.
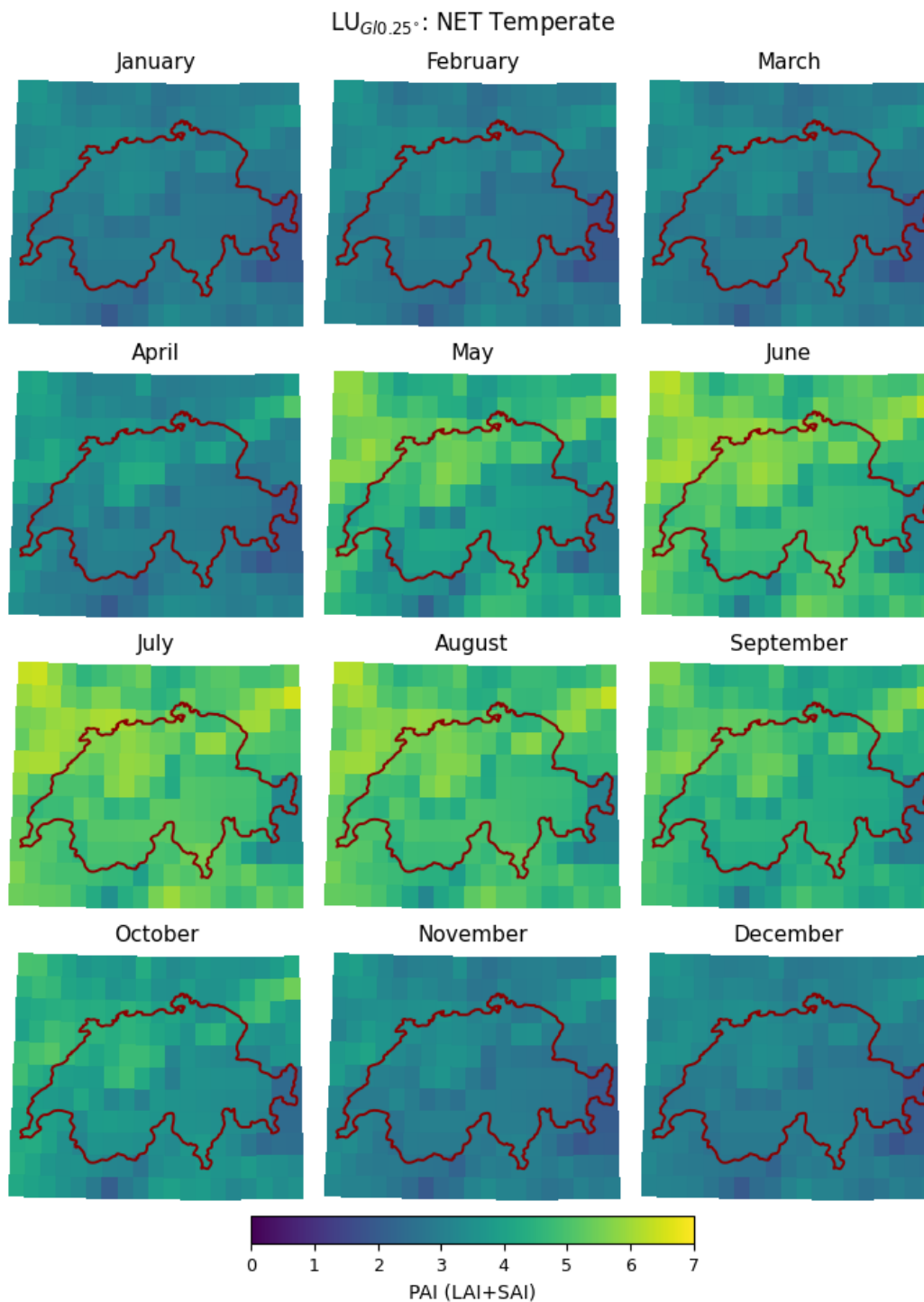
Figure B11. Monthly Plant Area Index (PAI) for temperate needle leaf evergreen trees for the global 0.25° land use dataset (LU$_{GI0.25°}$) as used in this study.
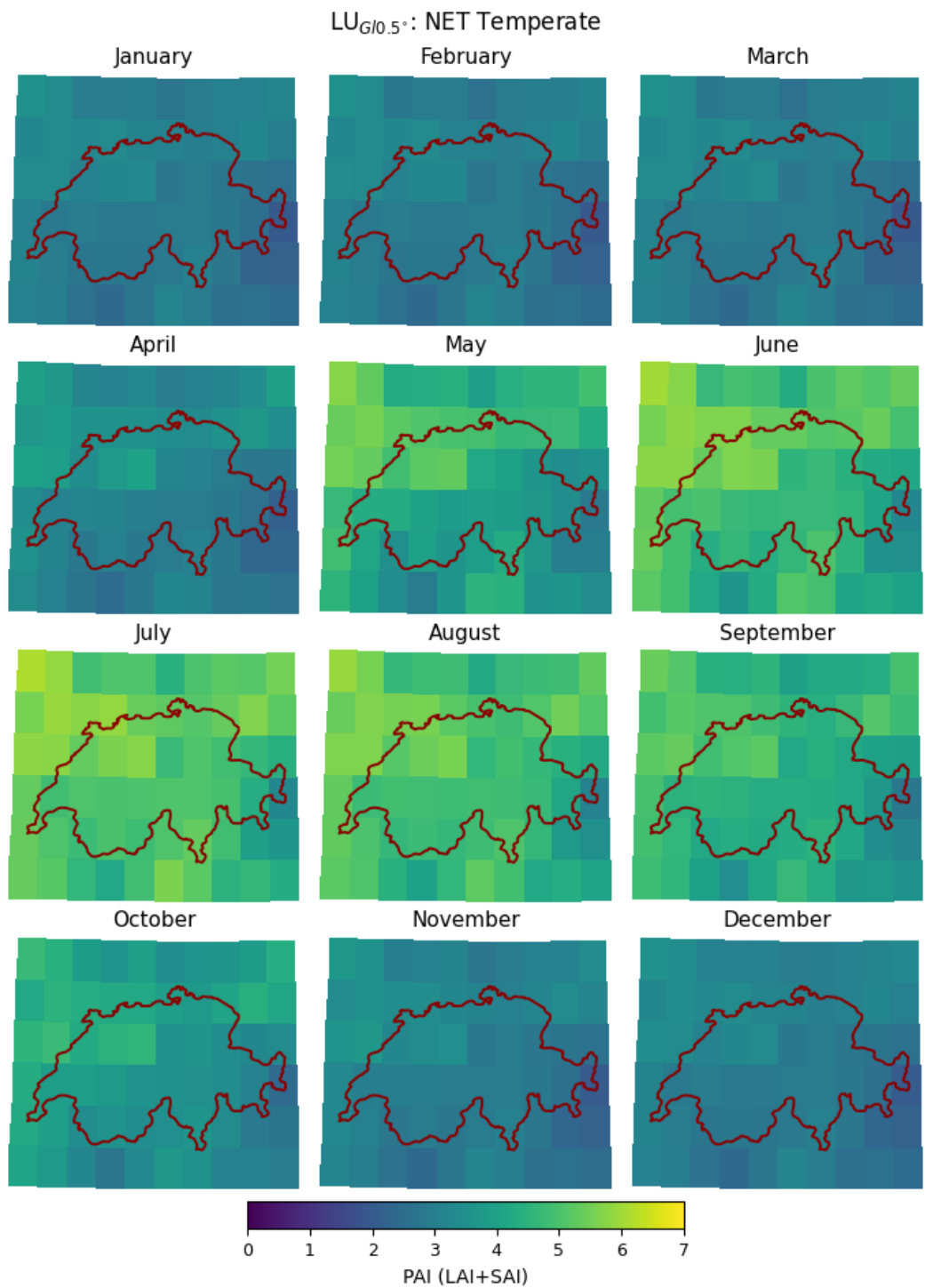
Figure B12. Monthly Plant Area Index (PAI) for temperate needle leaf evergreen trees for the global 0.5° land use dataset (LU$_{Gl0.5°}$) as used in this study.
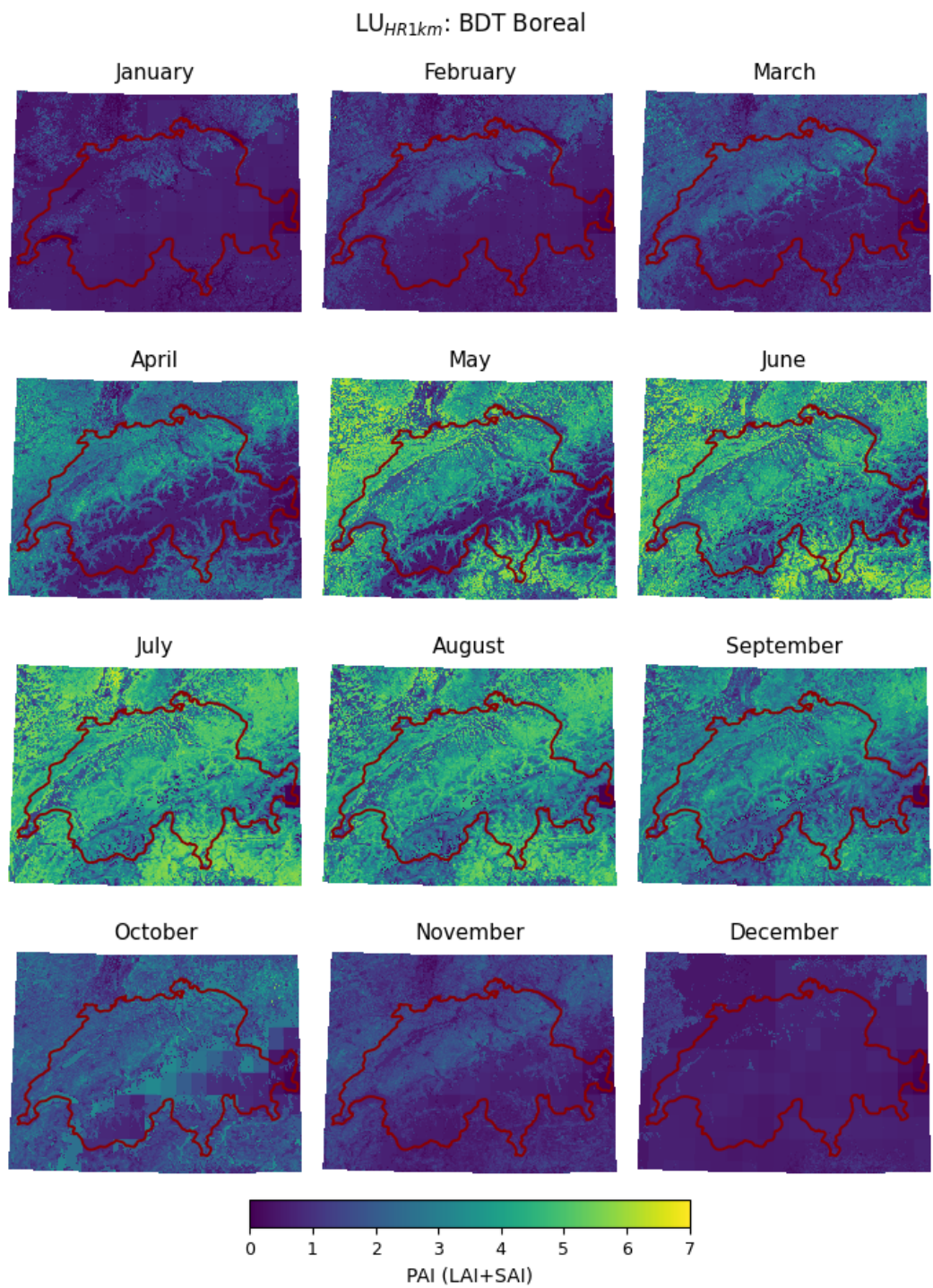
Figure B13. Monthly Plant Area Index (PAI) for boreal broad-leaf deciduous trees for the high-resolution 1km land use dataset (LU$_{HR1km}$) as used in this study.
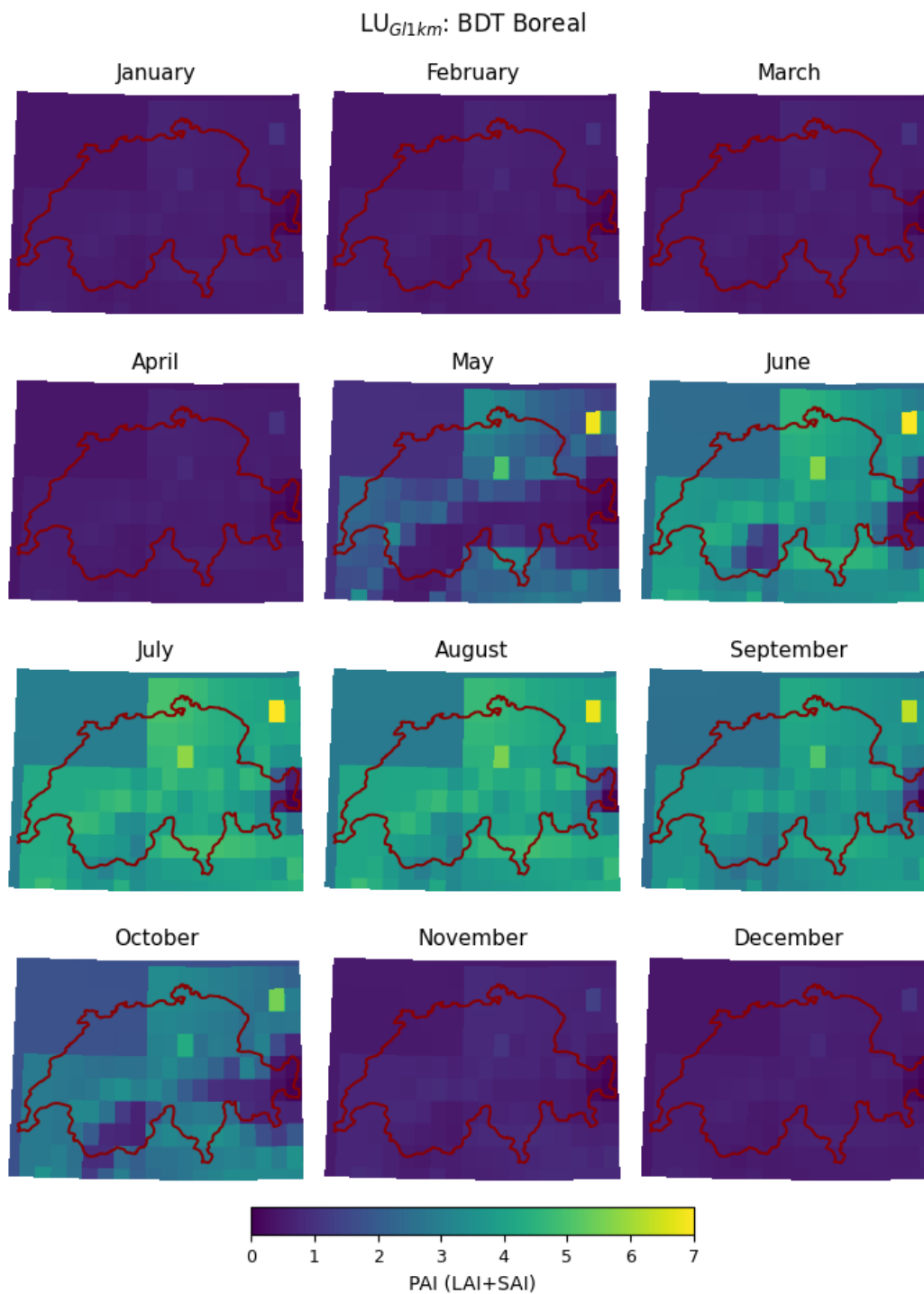
Figure B14. Monthly Plant Area Index (PAI) for boreal broad-leaf deciduous trees for the global 1km land use dataset (LU_{Gl1km}) as used in this study.
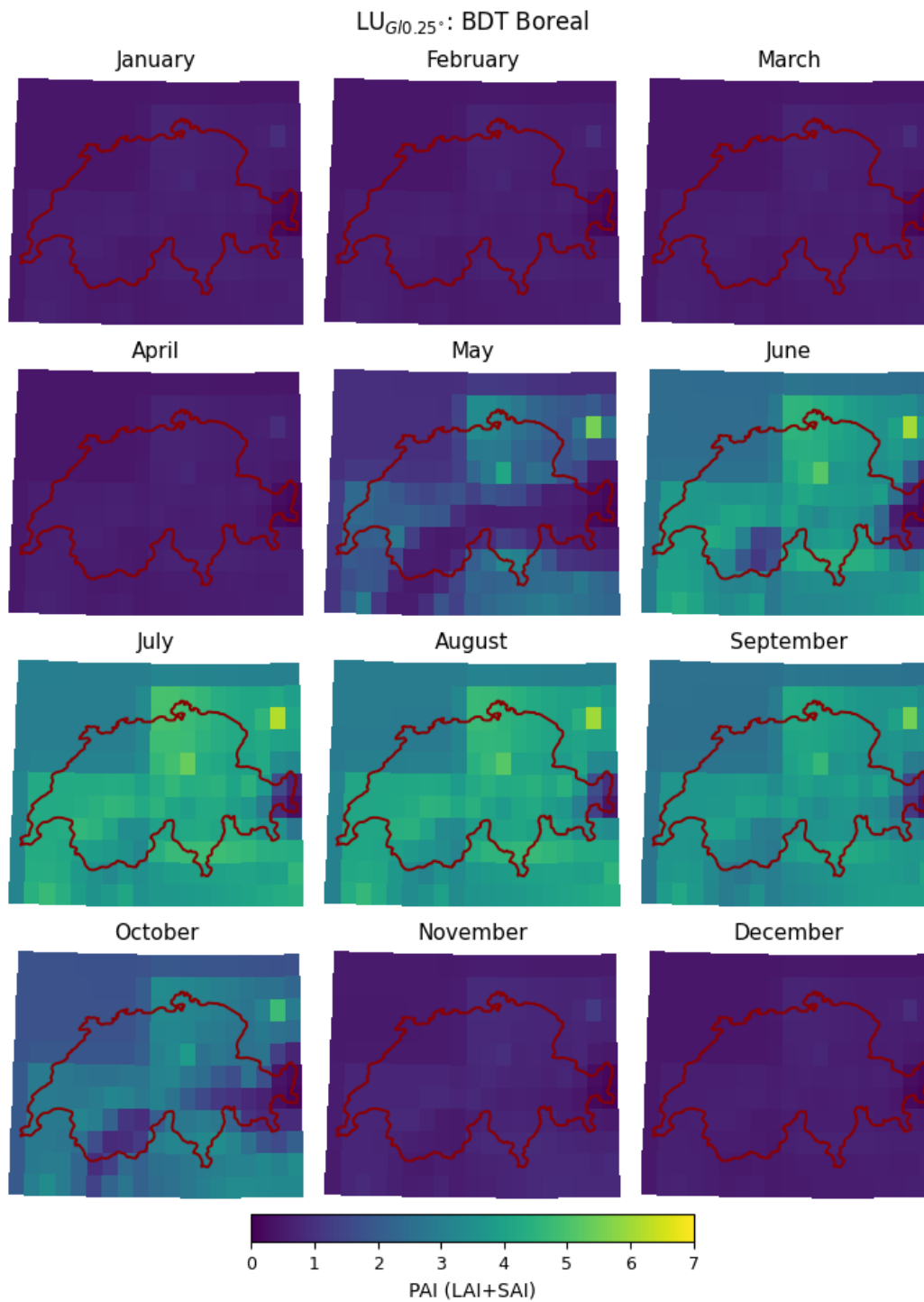
Figure B15. Monthly Plant Area Index (PAI) for boreal broad-leaf deciduous trees for the global 0.25° land use dataset (LU$_{GI0.25°}$) as used in this study.
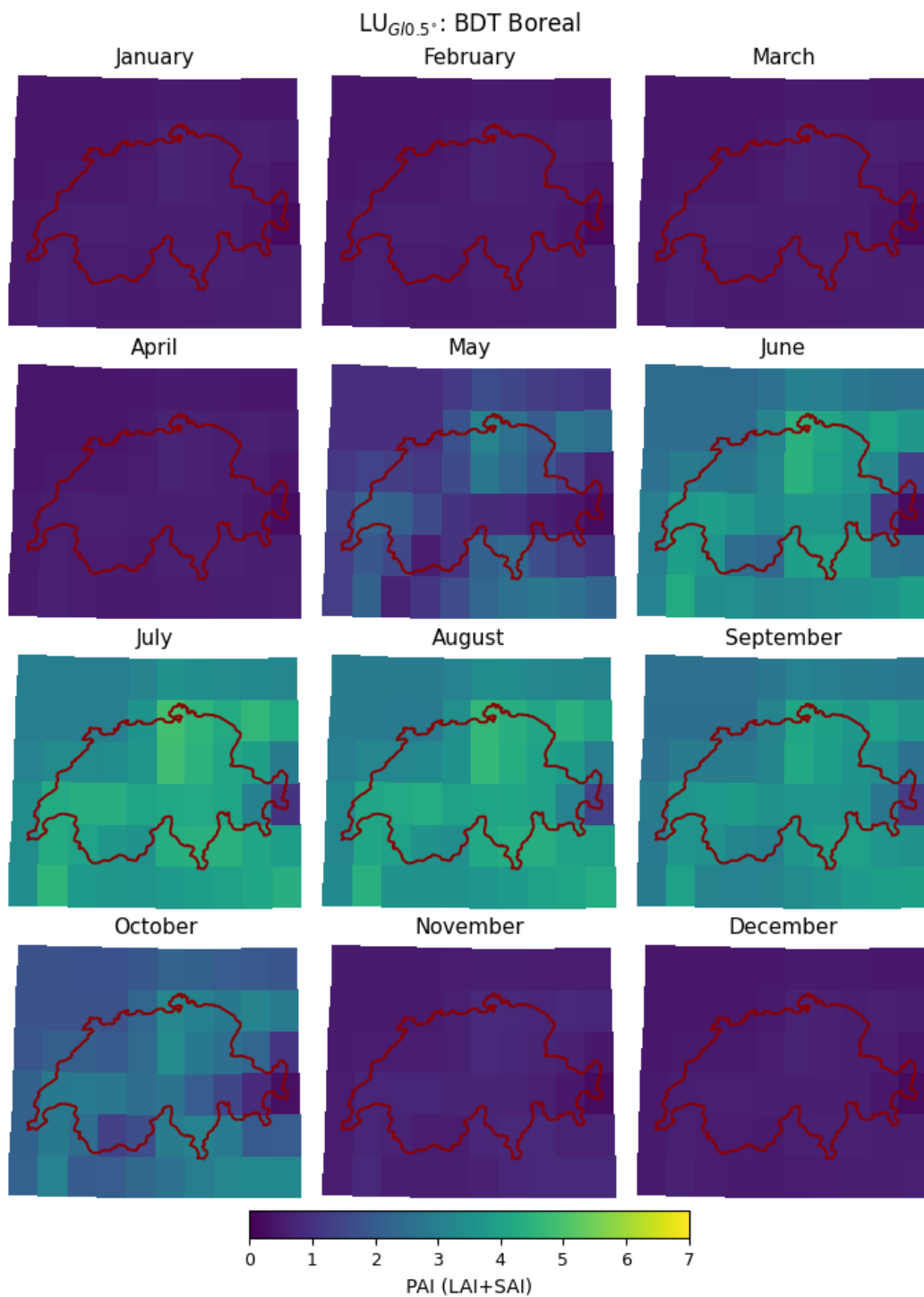
Figure B16. Monthly Plant Area Index (PAI) for boreal broad-leaf deciduous trees for the global 0.5° land use dataset (LU$_{GI0.5°}$) as used in this study.

Appendix C: Meteorological forcing data

This section shows supporting information regarding the meteorological forcing data presented in the main part of the manuscript.

545   First, we show the two DEMs used for lapse rate calculation in this study. We further show differences in yearly and monthly precipitation for the OSHD-based and CRU-based dataset, as well as differences in monthly temperatures between the OSHD-based, the CRU-based and the CRU* datset.
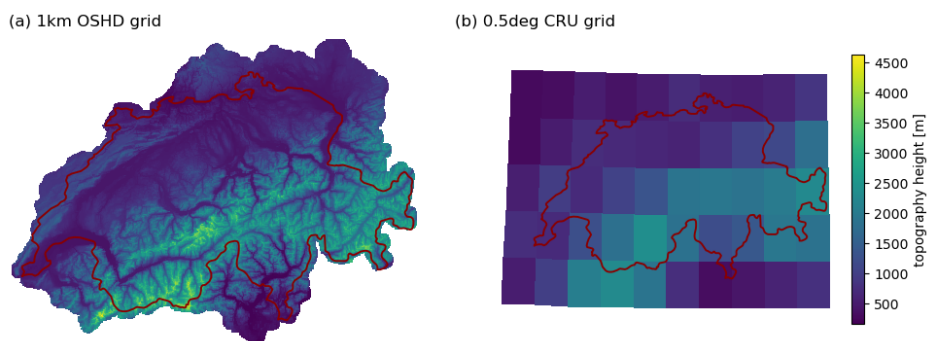
Figure C1. Comparison of digital elevation model (DEM) at (a) 1km and (b) 0.5°as used for lapse rate correction in this study.
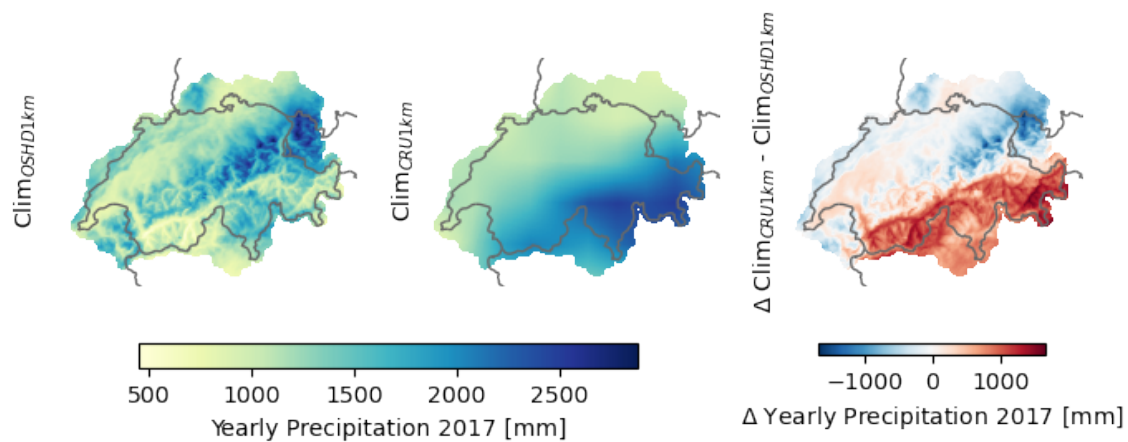
Figure C2. Total yearly precipitation input for the year 2017: OSHD-based, CRUJRA-based and a differential plot.
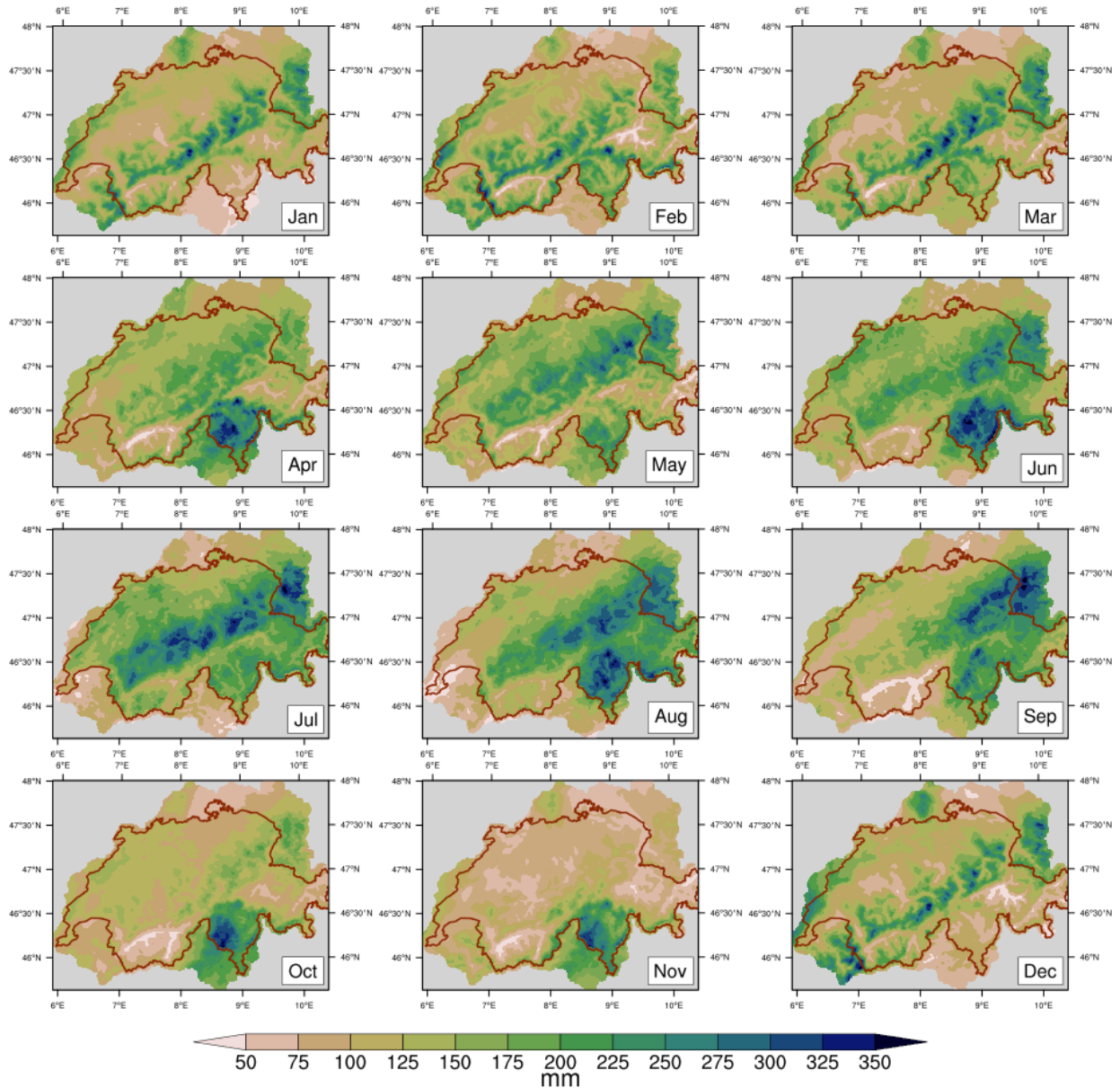
Figure C3. Total monthly precipitation input as averaged between 2014 and 2019 for the ClimOSHD forcing dataset.

Figure C4. Differences in total monthly precipitation input between the ClimOSHD and the ClimCRU forcing dataset.
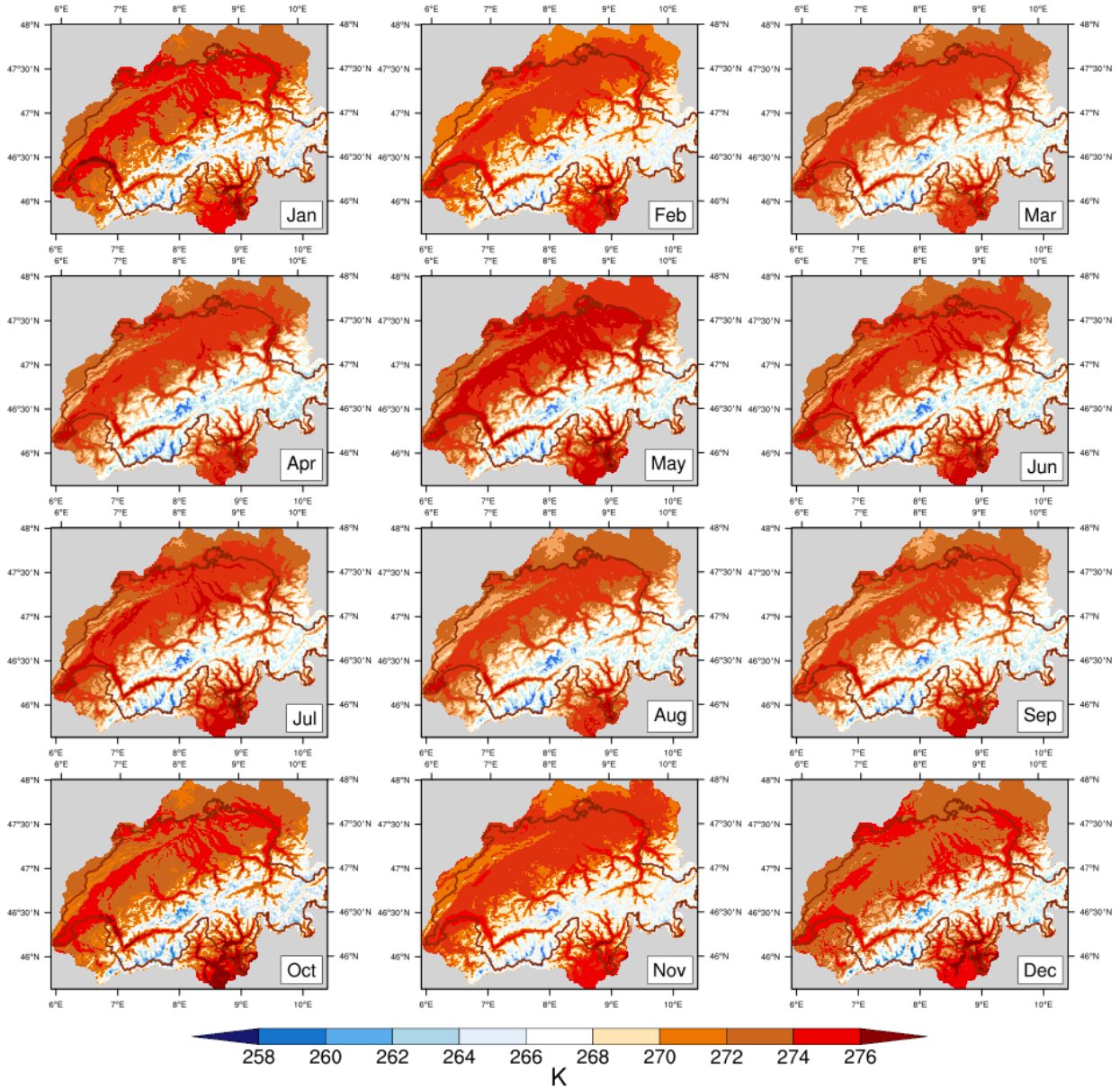
Figure C5. Mean monthly temperatures for the ClimOSHD forcing dataset.

Figure C6. Differences in mean monthly temperatures between the ClimOSHD and the ClimCRU forcing dataset.

Diff. in monthly mean temp (ClimOSHD-ClimCRU*, 2014-2019 mean)
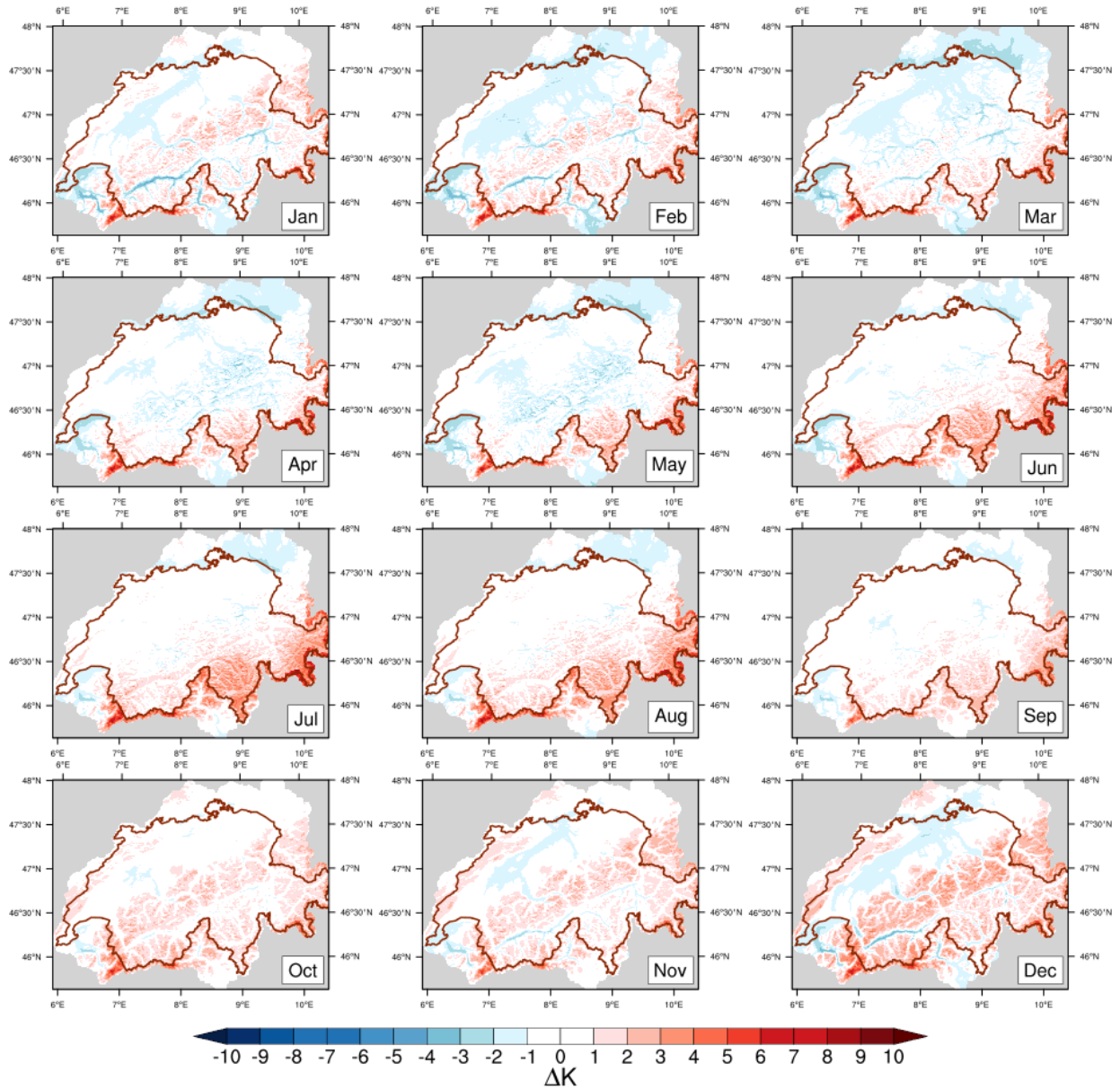
Figure C7. Differences in mean monthly temperatures between the ClimOSHD and the lapse-rate corrected ClimCRU* forcing dataset.

Appendix D: Spatially distributed CLM5 model simulations

This section shows supporting analyses for the spatially distributed CLM5 model simulations presented in the main part of the manuscript.
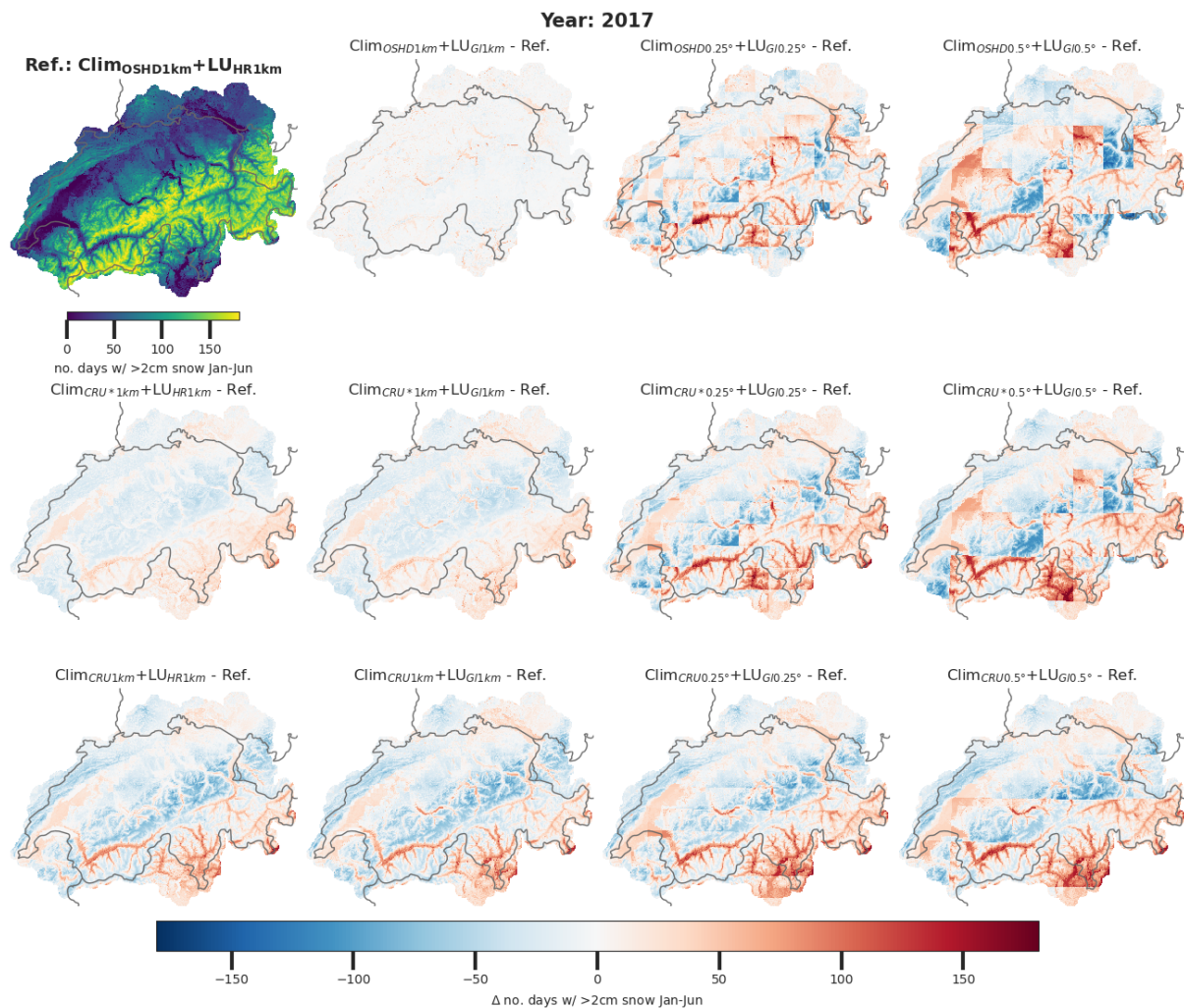
Figure D1. Spatial comparison of number of days with more than 2cm snow on the ground between January and June 2017: The reference case (Clim$_{OSHD1km}$+LU$_{HR1km}$) is compared with simulations of all other CLM5 configurations used in this study. For the residual plots, blue indicates underestimation and red indicates overestimation with regards to the reference case.
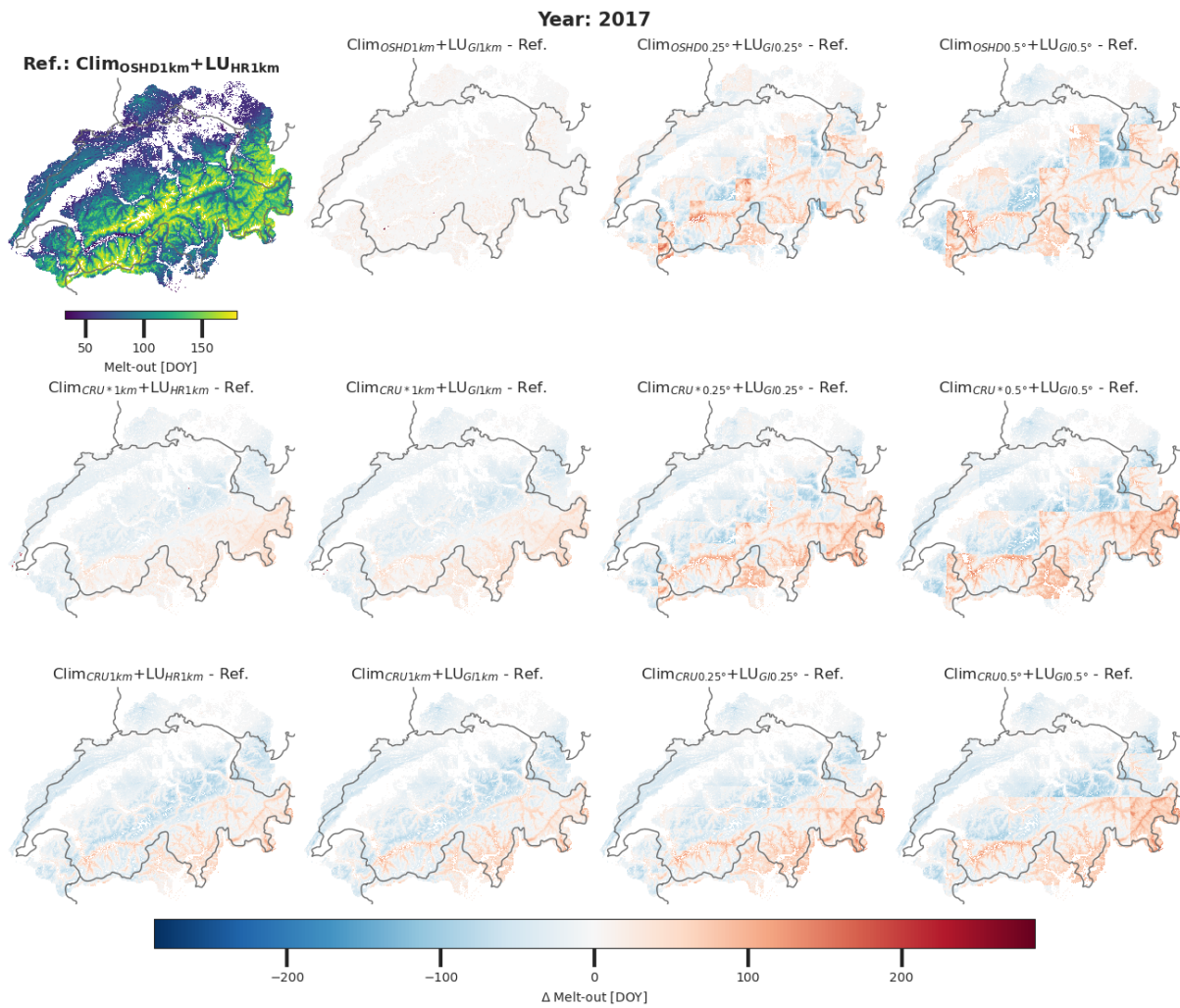
Figure D2. Spatial comparison of melt-out date (day of year) during 2017: The reference case (Clim$_{OSHD1km}$+LU$_{HR1km}$) is compared with simulations of all other CLM5 configurations used in this study. For the residual plots, blue indicates underestimation and red indicates overestimation with regards to the reference case.
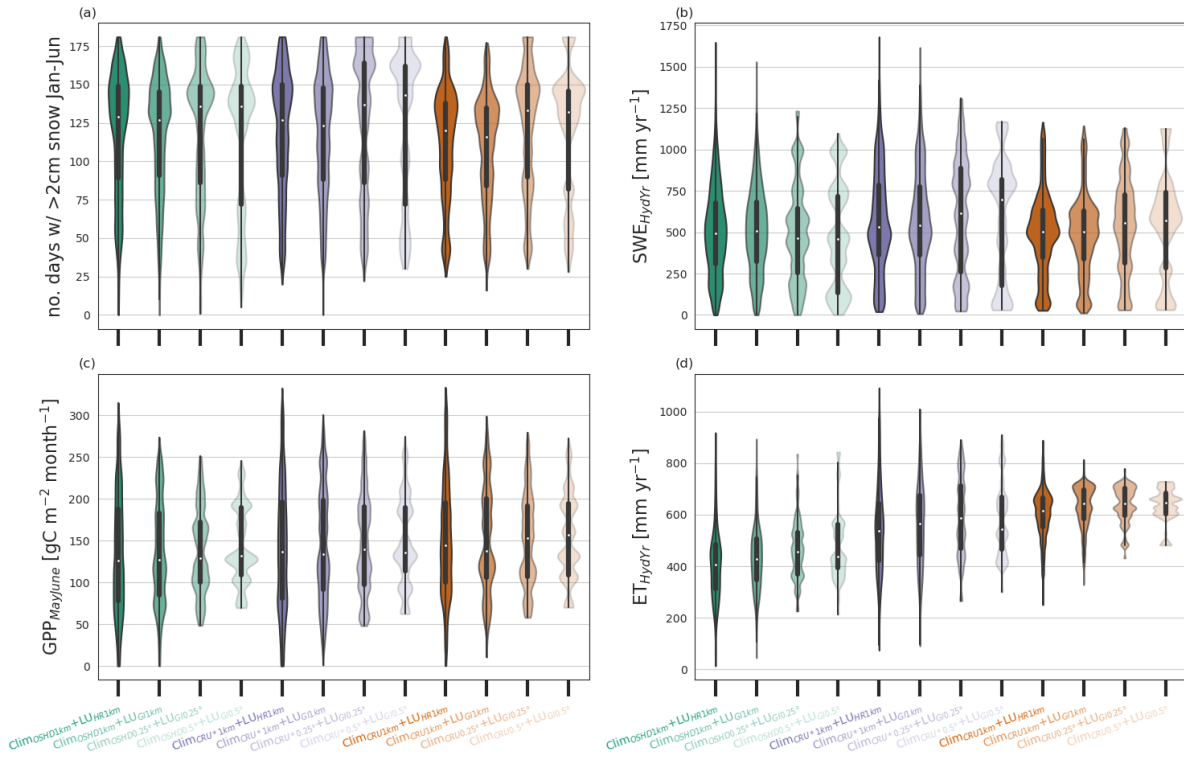
Figure D3. Violin-plots showing comparison of all 12 CLM5 model configurations for the year 2017 across the entire model domain: (a) number of days with >2cm of snow between January and June 2017, (b) cumulative SWE (total positive SWE increments; 'how much water is stored in total') during the hydrological year 2017 (1.10.2016 - 30.09.2017), (c) monthly-averaged GPP during May and June 2017and (d) total Evapotranspiration during the 2017 hydrological year. In addition to information obtained from a box plot (25th + 75th percentiles and median), the violin plots show a kernel density estimate of the data.

Author contributions. All authors helped design the experiments. JM set up the modelling infrastructure and performed the CLM5 simulations. JM performed the analysis, with input from all authors. JM wrote the manuscript, with contributions and feedback from all authors.

Competing interests. The authors declare that they have no conflict of interest.

Acknowledgements. The authors thank Thomas Kramer and his team for HPC support throughout this project. JM received funding from a WSL internal project call. DNK and JM were supported by the Swiss National Science Foundation SNF (project: Adohris, 205530), as was GM (project: P500PN, 202741). We further thank the team of the operational snow hydrologic service at SLF for providing input data. Developers of open source python toolboxes, particularly xarray (Hoyer and Hamman, 2017) and xesmf (Zhuang et al., 2023), have also played a crucial role in this study by enabling efficient analysis and manipulation of large datasets.

555

References

560 Ali, A. A., Xu, C., Rogers, A., Fisher, R. A., Wullschleger, S. D., Massoud, E. C., Vrugt, J. A., Muss, J. D., McDowell, N. G., Fisher, J. B., Reich, P. B., and Wilson, C. J.: A global scale mechanistic model of photosynthetic capacity (LUNA V1.0), Geoscientific Model Development, 9, 587–606, https://doi.org/10.5194/gmd-9-587-2016, 2016.

Anderson, E. A.: A Point Energy and Mass Balance Model of a Snow Cover, 1976.

Ban-Weiss, G. A., Bala, G., Cao, L., Pongratz, J., and Caldeira, K.: Climate forcing and response to idealized changes in surface latent and
565 sensible heat, Environmental Research Letters, 6, https://doi.org/10.1088/1748-9326/6/3/034032, 2011.

Barnett, T. P., Adam, J. C., and Lettenmaier, D. P.: Potential impacts of a warming climate on water availability in snow-dominated regions., Nature, 438, 303–309, https://doi.org/10.1038/nature04141, barnett, T P
Adam, J C
Lettenmaier, D P
eng
Research Support, U.S. Gov't, Non-P.H.S.
England
2005/11/18 09:00
Nature. 2005 Nov 17;438(7066):303-9., 2005.

Bartelt, P. and Lehning, M.: A physical SNOWPACK model for the Swiss avalanche warning Part I: numerical model, Cold Regions Science
570 and Technology, 35, 123–145, www.elsevier.com/locate/coldregions, 2002.

Beven, K. J. and Cloke, H. L.: Comment on "Hyperresolution global land surface modeling: Meeting a grand challenge for monitoring Earth's terrestrial water" by Eric F. Wood et al., Water Resources Research, 48, 2–4, https://doi.org/10.1029/2011wr010982, 2012.

Blyth, E. M., Arora, V. K., Clark, D. B., Dadson, S. J., Kauwe, M. G. D., Lawrence, D. M., Melton, J. R., Pongratz, J., Turton, R. H., Yoshimura, K., and Yuan, H.: Advances in Land Surface Modelling, Current Climate Change Reports, 7, 45–71,
575 https://doi.org/10.1007/s40641-021-00171-5, 2021.

Bonan, G. B., Lawrence, P. J., Oleson, K. W., Levis, S., Jung, M., Reichstein, M., Lawrence, D. M., and Swenson, S. C.: Improving canopy processes in the Community Land Model version 4 (CLM4) using global flux fields empirically inferred from FLUXNET data, Journal of Geophysical Research, 116, 1–22, https://doi.org/10.1029/2010jg001593, 2011.

Boone, A. A. and Etchevers, P.: An intercomparison of three snow schemes of varying complexity coupled to the same land
580 surface model: Local-scale evaluation at an alpine site, Journal of Hydrometeorology, 2, 374–394, https://doi.org/10.1175/1525-7541(2001)002<0374:AIOTSS>2.0.CO;2, 2001.

Ciscar, J. C., Rising, J., Kopp, R. E., and Feyen, L.: Assessing future climate change impacts in the EU and the USA: Insights and lessons from two continental-scale projects, Environmental Research Letters, 14, https://doi.org/10.1088/1748-9326/ab281e, 2019.

Clark, M. P., Hendrikx, J., Slater, A. G., Kavetski, D., Anderson, B., Cullen, N. J., Kerr, T., Örn Hreinsson, E., and Woods, R. A.: Representing
585 spatial variability of snow water equivalent in hydrologic and land-surface models: A review, https://doi.org/10.1029/2011WR010745, 2011.

Dai, Y. and Zeng, Q.: A Land Surface Model (IAP94) for Climate Studies Part I: Formulation and Validation in Off-line Experiments, Advances in Atmospheric Sciences, 14, 1997.

Dirmeyer, P. A., Gao, X., Zhao, M., Guo, Z., Oki, T., and Hanasaki, N.: GSWP-2: Multimodel analysis and implications for our perception
590 of the land surface, Bulletin of the American Meteorological Society, 87, 1381–1397, https://doi.org/10.1175/BAMS-87-10-1381, 2006.

Douville, H., Royer, J.-F., and Mahfouf, J.-F.: A new snow parameterization for the M6t o-France climate model Part I: validation in stand-alone experiments, Climate Dynamics, 12, 21–35, https://doi.org/10.1007/BF00208760, 1995.

Dutra, E., Viterbo, P., Miranda, P. M. A., and Balsamo, G.: American Meteorological Society Complexity of Snow Schemes in a Climate Model and Its Impact on Surface Energy and Hydrology, Source: Journal of Hydrometeorology, 13, 521–538,
595 https://doi.org/10.2307/24912781, 2012.

Essery, R.: Aggregated and distributed modelling of snow cover for a high-latitude basin, Global and Planetary Change, 38, 115–120, https://doi.org/10.1016/S0921-8181(03)00013-4, 2003.

Essery, R.: A factorial snowpack model (FSM 1.0), Geoscientific Model Development, 8, 3867–3876, https://doi.org/10.5194/gmd-8-3867-2015, 2015.

600 Essery, R., Morin, S., Lejeune, Y., and Ménard, C. B.: A comparison of 1701 snow models using observations from an alpine site, Advances in Water Resources, 55, 131–148, https://doi.org/10.1016/j.advwatres.2012.07.013, 2013.

Farquhar, G. D., Caemmerer, S., and Berry, J. A.: A biochemical model of photosynthetic CO_2 assimilation in leaves of C_3 species, Planta, 149, 78–90–90, http://dx.doi.org/10.1007/BF00386231, 1980.

Ferguson, C. R., Wood, E. F., and Vinukollu, R. K.: A Global intercomparison of modeled and observed land-atmosphere coupling, Journal 605 of Hydrometeorology, 13, 749–784, https://doi.org/10.1175/JHM-D-11-0119.1, 2012.

Fisher, R. A. and Koven, C. D.: Perspectives on the Future of Land Surface Models and the Challenges of Representing Complex Terrestrial Systems, Journal of Advances in Modeling Earth Systems, 12, https://doi.org/10.1029/2018MS001453, 2020.

Fisher, R. A., Wieder, W. R., Sanderson, B. M., Koven, C. D., Oleson, K. W., Xu, C., Fisher, J. B., Shi, M., Walker, A. P., and Lawrence, D. M.: Parametric Controls on Vegetation Responses to Biogeochemical Forcing in the CLM5, Journal of Advances in Modeling Earth 610 Systems, 11, 2879–2895, https://doi.org/10.1029/2019MS001609, 2019.

Flanner, M. G. and Zender, C. S.: Snowpack radiative heating: Influence on Tibetan Plateau climate, Geophysical Research Letters, 32, 1–5, https://doi.org/10.1029/2004GL022076, 2005.

Flanner, M. G., Shell, K. M., Barlage, M., Perovich, D. K., and Tschudi, M. A.: Radiative forcing and albedo feedback from the Northern Hemisphere cryosphere between 1979 and 2008, Nature Geoscience, 4, 151–155, https://doi.org/10.1038/ngeo1062, 2011.

615 Friedlingstein, P., O'Sullivan, M., Jones, M. W., Andrew, R. M., Hauck, J., Olsen, A., Peters, G. P., Peters, W., Pongratz, J., Sitch, S., Quéré, C. L., Canadell, J. G., Ciais, P., Jackson, R. B., Alin, S., Aragão, L. E., Arneth, A., Arora, V., Bates, N. R., Becker, M., Benoit-Cattin, A., Bittig, H. C., Bopp, L., Bultan, S., Chandra, N., Chevallier, F., Chini, L. P., Evans, W., Florentie, L., Forster, P. M., Gasser, T., Gehlen, M., Gilfillan, D., Gkritzalis, T., Gregor, L., Gruber, N., Harris, I., Hartung, K., Haverd, V., Houghton, R. A., Ilyina, T., Jain, A. K., Joetzjer, E., Kadono, K., Kato, E., Kitidis, V., Korsbakken, J. I., Landschützer, P., Lefèvre, N., Lenton, A., Lienert, S., Liu, Z., Lombardozzi, D., 620 Marland, G., Metzl, N., Munro, D. R., Nabel, J. E., Nakaoka, S. I., Niwa, Y., O'Brien, K., Ono, T., Palmer, P. I., Pierrot, D., Poulter, B., Resplandy, L., Robertson, E., Rödenbeck, C., Schwinger, J., Séférian, R., Skjelvan, I., Smith, A. J., Sutton, A. J., Tanhua, T., Tans, P. P., Tian, H., Tilbrook, B., Werf, G. V. D., Vuichard, N., Walker, A. P., Wanninkhof, R., Watson, A. J., Willis, D., Wiltshire, A. J., Yuan, W., Yue, X., and Zaehle, S.: Data used with permission of the Global Carbon Project under the Creative Commons Attribution 4.0 International license, Earth System Science Data, 12, 3269–3340, 2020.

625 Griessinger, N., Schirmer, M., Helbig, N., Winstral, A., Michel, A., and Jonas, T.: Implications of observation-enhanced energy-balance snowmelt simulations for runoff modeling of Alpine catchments, Advances in Water Resources, 133, 103 410, https://doi.org/10.1016/j.advwatres.2019.103410, 2019.

Harris, I., Jones, P. D., Osborn, T. J., and Lister, D. H.: Updated high-resolution grids of monthly climatic observations - the CRU TS3.10 Dataset, International Journal of Climatology, 34, 623–642, https://doi.org/10.1002/joc.3711, 2014.

630 Hoyer, S. and Hamman, J.: xarray: N-D labeled Arrays and Datasets in Python, Journal of Open Research Software, 5, 10, https://doi.org/10.5334/jors.148, 2017.

Hurk, B. V. D., Kim, H., Krinner, G., Seneviratne, S. I., Derksen, C., Oki, T., Douville, H., Colin, J., Ducharne, A., Cheruy, F., Viovy, N., Puma, M. J., Wada, Y., Li, W., Jia, B., Alessandri, A., Lawrence, D. M., Weedon, G. P., Ellis, R., Hagemann, S., Mao, J., Flanner,

M. G., Zampieri, M., Materia, S., Law, R. M., and Sheffield, J.: LS3MIP (v1.0) contribution to CMIP6: The Land Surface, Snow and Soil moisture Model Intercomparison Project - Aims, setup and expected outcome, Geoscientific Model Development, 9, 2809–2832, https://doi.org/10.5194/gmd-9-2809-2016, 2016.

IPCC: Climate Change 2022: Impacts, Adaptation, and Vulnerability. Contribution of Working Group II to the Sixth Assessment Report of the Intergovernmental Panel on Climate Change, Cambridge University Press, 2022.

Jonas, T., Rixen, C., Sturm, M., and Stoeckli, V.: How alpine plant growth is linked to snow cover and climate variability, Journal of Geophysical Research: Biogeosciences, 113, https://doi.org/10.1029/2007JG000680, 2008.

Jordan, R.: A One-Dimensional Temperature Model for a Snow Cover: Technical Documentation for SNTHERM.89, 1991.

Kobayashi, S., Ota, Y., Harada, Y., Ebita, A., Moriya, M., Onoda, H., Onogi, K., Kamahori, H., Kobayashi, C., Endo, H., Miyaoka, K., and Kiyotoshi, T.: The JRA-55 reanalysis: General specifications and basic characteristics, Journal of the Meteorological Society of Japan, 93, 5–48, https://doi.org/10.2151/jmsj.2015-001, 2015.

Lawrence, D. M., Thornton, P. E., Oleson, K. W., and Bonan, G. B.: The partitioning of evapotranspiration into transpiration, soil evaporation, and canopy evaporation in a GCM: Impacts on land-atmosphere interaction, Journal of Hydrometeorology, 8, 862–880, https://doi.org/10.1175/JHM596.1, 2007.

Lawrence, D. M., Fisher, R. A., Koven, C., Oleson, K. W., Swenson, S. C., and Vertenstein, M.: Technical Description of version 5.0 of the Community Land Model (CLM), 2018.

Lawrence, D. M., Fisher, R. A., Koven, C. D., Oleson, K. W., Swenson, S. C., Bonan, G., Collier, N., Ghimire, B., van Kampenhout, L., Kennedy, D., Kluzek, E., Lawrence, P. J., Li, F., Li, H., Lombardozzi, D., Riley, W. J., Sacks, W. J., Shi, M., Vertenstein, M., Wieder, W. R., Xu, C., Ali, A. A., Badger, A. M., Bisht, G., van den Broeke, M., Brunke, M. A., Burns, S. P., Buzan, J., Clark, M., Craig, A., Dahlin, K., Drewniak, B., Fisher, J. B., Flanner, M., Fox, A. M., Gentine, P., Hoffman, F., Keppel-Aleks, G., Knox, R., Kumar, S., Lenaerts, J., Leung, L. R., Lipscomb, W. H., Lu, Y., Pandey, A., Pelletier, J. D., Perket, J., Randerson, J. T., Ricciuto, D. M., Sanderson, B. M., Slater, A., Subin, Z. M., Tang, J., Thomas, R. Q., Martin, M. V., and Zeng, X.: The Community Land Model Version 5: Description of New Features, Benchmarking, and Impact of Forcing Uncertainty, Journal of Advances in Modeling Earth Systems, 11, 4245–4287, https://doi.org/10.1029/2018MS001583, 2019.

Lawrence, P. J. and Chase, T. N.: Representing a new MODIS consistent land surface in the Community Land Model (CLM 3.0), Journal of Geophysical Research: Biogeosciences, 112, https://doi.org/10.1029/2006JG000168, 2007.

Lei, Y., Pan, J., Xiong, C., Jiang, L., and Shi, J.: Snow depth and snow cover over the Tibetan Plateau observed from space in against ERA5: matters of scale, Climate Dynamics, https://doi.org/10.1007/s00382-022-06376-0, 2022.

Lüthi, S., Ban, N., Kotlarski, S., Steger, C. R., Jonas, T., and Schär, C.: Projections of Alpine snow-cover in a high-resolution climate simulation, Atmosphere, 10, 1–18, https://doi.org/10.3390/atmos10080463, 2019.

Ma, X. and Wang, A.: Systematic Evaluation of a High-Resolution CLM5 Simulation over Continental China for 1979-2018, Journal of Hydrometeorology, 23, 1879 –1897, https://doi.org/10.1175/JHM-D-22, 2022.

Magnusson, J., Gustafsson, D., Huesler, F., and Jonas, T.: Assimilation of point SWE data into a distributed snow cover model comparing two contrasting methods, Water Resources Research, 50, 7816–7835, https://doi.org/10.1002/2013WR014792.Received, 2014.

Magnusson, J., Wever, N., Essery, R., Helbig, N., Winstral, A., and Jonas, T.: Evaluating snow models with varying process representations for hydrological applications, Water Resources Research, 51, 2707–2723, https://doi.org/10.1002/2014WR016498, 2015.

670   Magnusson, J., Eisner, S., Huang, S., Lussana, C., Mazzotti, G., Essery, R., Saloranta, T., and Beldring, S.: Influence of Spatial Resolution on Snow Cover Dynamics for a Coastal and Mountainous Region at High Latitudes (Norway), Water Resources Research, 55, 5612–5630, https://doi.org/10.1029/2019WR024925, 2019.

Male, D. H. and Granger, R. J.: Snow surface energy exchange, Water Resour. Res., 17, 609–627, https://doi.org/10.1029/WR017i003p00609, 1981.

675   Mankin, J. S., Viviroli, D., Singh, D., Hoekstra, A. Y., and Diffenbaugh, N. S.: The potential for snow to supply human water demand in the present and future, Environmental Research Letters, 10, 114 016, https://doi.org/10.1088/1748-9326/10/11/114016, 2015.

Mazzotti, G., Essery, R., Webster, C., Malle, J., and Jonas, T.: Process-Level Evaluation of a Hyper-Resolution Forest Snow Model Using Distributed Multisensor Observations, Water Resources Research, 56, https://doi.org/10.1029/2020WR027572, 2020.

Mazzotti, G., Webster, C., Essery, R., and Jonas, T.: Increasing the Physical Representation of Forest-Snow Processes in
680   Coarse-Resolution Models: Lessons Learned From Upscaling Hyper-Resolution Simulations, Water Resources Research, 57, https://doi.org/10.1029/2020WR029064, 2021.

Meissner, C., Schädler, G., Panitz, H. J., Feldmann, H., and Kottmeier, C.: High-resolution sensitivity studies with the regional climate model COSMO-CLM, Meteorologische Zeitschrift, 18, 543–557, https://doi.org/10.1127/0941-2948/2009/0400, 2009.

Mott, R., Winstral, A., Cluzet, B., Helbig, N., Magnusson, J., Mazzotti, G., Quéno, L., Schirmer, M., Webster, C., and Jonas, T.: Operational
685   snow-hydrological modeling for Switzerland, Frontiers in Earth Science, 11, https://doi.org/10.3389/feart.2023.1228158, 2023.

Niu, G. Y., Yang, Z. L., Mitchell, K. E., Chen, F., Ek, M. B., Barlage, M., Kumar, A., Manning, K., Niyogi, D., Rosero, E., Tewari, M., and Xia, Y.: The community Noah land surface model with multiparameterization options (Noah-MP): 1. Model description and evaluation with local-scale measurements, Journal of Geophysical Research Atmospheres, 116, https://doi.org/10.1029/2010JD015139, 2011.

of East Anglia Climatic Research Unit; Harris, I. U.: CRU JRA v2.0: A forcings dataset of gridded land surface blend of Climatic Re-
690   search Unit (CRU) and Japanese reanalysis (JRA) data; Jan.1901 - Dec.2018.. Centre for Environmental Data Analysis, 08.06.2022. https://catalogue.ceda.ac.uk/, Norwich: University of East Anglia, 2019.

Oleson, K. W., Lawrence, D. M., Gordon, B., Flanner, M. G., Kluzek, E., Peter, J., Levis, S., Swenson, S. C., Thornton, E., Dai, A., Decker, M., Dickinson, R., Feddema, J., Heald, C. L., Lamarque, J.-F., yue Niu, G., Qian, T., Running, S., Sakaguchi, K., Slater, A., Stöckli, R., Wang, A., Yang, L., Zeng, X. X., Zeng, X. X., Bonan, G. B., Flanner, M. G., Kluzek, E., Lawrence, P. J., Levis, S., Swenson, S. C.,
695   Thornton, P. E., Dai, A., Decker, M., Dickinson, R., Feddema, J., Heald, C. L., Hoffman, F., Lamarque, J.-F., Mahowald, N., yue Niu, G., Qian, T., Randerson, J., Running, S., Sakaguchi, K., Slater, A., Stöckli, R., Wang, A., Yang, Z.-L., Zeng, X. X., and Zeng, X. X.: Technical Description of version 4 . 0 of the Community Land Model (CLM), http://www.ucar.edu/library/collections/technotes/technotes.jsp, 2010.

Pachauri, R. K., Allen, M. R., Barros, V. R., Broome, J., Cramer, W., Christ, R., Church, J. A., Clarke, L., Dahe, Q., Dasgupta, P., Dubash, N. K., Edenhofer, O., Elgizouli, I., Field, C. B., Forster, P., Friedlingstein, P., Fuglestvedt, J., Gomez-Echeverri, L., Hallegatte, S., Hegerl,
700   G., Howden, M., Jiang, K., Cisneroz, B. J., Kattsov, V., Lee, H., Mach, K. J., Marotzke, J., Mastrandrea, M. D., Meyer, L., Minx, J., Mulugetta, Y., O'Brien, K., Oppenheimer, M., Pereira, J. J., Pichs-Madruga, R., Plattner, G.-K., Pörtner, H.-O., Power, S. B., Preston, B., Ravindranath, N. H., Reisinger, A., Riahi, K., Rusticucci, M., Scholes, R., Seyboth, K., Sokona, Y., Stavins, R., Stocker, T. F., Tschakert, P., van Vuuren, D., and van Ypserle, J.-P.: Climate Change 2014: Synthesis Report. Contribution of Working Groups I, II and III to the Fifth Assessment Report of the Intergovernmental Panel on Climate Change, IPCC, 2014.

705   Peters-Lidard, C. D., Mocko, D. M., Garcia, M., Santanello, J. A., Tischler, M. A., Moran, M. S., and Wu, Y.: Role of precipitation uncertainty in the estimation of hydrologic soil properties using remotely sensed soil moisture in a semiarid environment, Water Resources Research, 44, 1–22, https://doi.org/10.1029/2007WR005884, 2008.

Pritchard, H. D.: Asia's shrinking glaciers protect large populations from drought stress, Nature, 569, 649–654, https://doi.org/10.1038/s41586-019-1240-1, 2019.

710 Qin, Y., Abatzoglou, J. T., Siebert, S., Huning, L. S., AghaKouchak, A., Mankin, J. S., Hong, C., Tong, D., Davis, S. J., and Mueller, N. D.: Agricultural risks from changing snowmelt, Nature Climate Change, 10, 459–465, https://doi.org/10.1038/s41558-020-0746-8, 2020.

Ridder, N. N., Pitman, A. J., and Ukkola, A. M.: Do CMIP6 Climate Models Simulate Global or Regional Compound Events Skillfully?, Geophysical Research Letters, 48, 1–11, https://doi.org/10.1029/2020GL091152, 2021.

Rimal, B., Sharma, R., Kunwar, R., Keshtkar, H., Stork, N. E., Rijal, S., Rahman, S. A., and Baral, H.: Effects of land
715 use and land cover change on ecosystem services in the Koshi River Basin, Eastern Nepal, Ecosystem Services, 38, https://doi.org/10.1016/j.ecoser.2019.100963, 2019.

Schär, C., Fuhrer, O., Arteaga, A., Ban, N., Charpilloz, C., Girolamo, S. D., Hentgen, L., Hoefler, T., Lapillonne, X., Leutwyler, D., Osterried, K., Panosetti, D., Rüdisühli, S., Schlemmer, L., Schulthess, T. C., Sprenger, M., Ubbiali, S., and Wernli, H.: Kilometer-scale climate models: Prospects and challenges, Bulletin of the American Meteorological Society, 101, E567–E587, https://doi.org/10.1175/BAMS-D-
720 18-0167.1, 2020.

Seneviratne, S. I., Lüthi, D., Litschi, M., and Schär, C.: Land-atmosphere coupling and climate change in Europe, Nature, 443, 205–209, https://doi.org/10.1038/nature05095, 2006.

Shrestha, B., Zhang, L., Sharma, S., Shrestha, S., and Khadka, N.: Effects on ecosystem services value due to land use and land cover change (1990–2020) in the transboundary Karnali River Basin, Central Himalayas, SN Applied Sciences, 4, https://doi.org/10.1007/s42452-022-
725 05022-y, 2022.

Singh, R. S., Reager, J. T., Miller, N. L., and Famiglietti, J. S.: Toward hyper-resolution land-surface modeling: The effects of fine-scale topography and soil texture on CLM4.0 simulations over the Southwestern U.S., Water Resources Research, 51, 2648–2667, https://doi.org/10.1002/2014WR015686, 2015.

Slatyer, R. A., Umbers, K. D., and Arnold, P. A.: Ecological responses to variation in seasonal snow cover,
730 https://doi.org/10.1111/cobi.13727, 2022.

Swenson, S. C. and Lawrence, D. M.: A new fractional snow-covered area parameterization for the Community Land Model and its effect on the surface energy balance, Journal of Geophysical Research Atmospheres, 117, 1–20, https://doi.org/10.1029/2012JD018178, 2012.

Swiss-Federal-Statistical-Office: Waldmischungsgrad, Auflösung 100m: Geodaten, https://dam-api.bfs.admin.ch/hub/api/dam/assets/860862/master, 2013.

735 Taylor, K. E.: Summarizing multiple aspects of model performance in a single diagram, Journal of Geophysical Research: Atmospheres, 106, 7183–7192, https://doi.org/https://doi.org/10.1029/2000JD900719, 2001.

Thackeray, C. W. and Fletcher, C. G.: Snow albedo feedback: Current knowledge, importance, outstanding issues and future directions, Progress in Physical Geography, 40, 392–408, https://doi.org/10.1177/0309133315620999, 2016.

Thackeray, C. W., Derksen, C., Fletcher, C. G., and Hall, A.: Snow and Climate: Feedbacks, Drivers, and Indices of Change, Current Climate
740 Change Reports, 5, 322–333, https://doi.org/10.1007/s40641-019-00143-w, 2019.

Thornton, P. E. and Zimmermann, N. E.: An improved canopy integration scheme for a Land Surface Model with prognostic canopy structure, Journal of Climate, 20, 3902–3923, https://doi.org/10.1175/JCLI4222.1, 2007.

Tsendbazar, N., Herold, M., Li, L., Tarko, A., de Bruin, S., Masiliunas, D., Lesiv, M., Fritz, S., Buchhorn, M., Smets, B., Kerchove, R. V. D., and Duerauer, M.: Towards operational validation of annual global land cover maps, Remote Sensing of Environment, 266,
745 https://doi.org/10.1016/j.rse.2021.112686, 2021.

van Kampenhout, L., Lenaerts, J. T., Lipscomb, W. H., Sacks, W. J., Lawrence, D. M., Slater, A. G., and van den Broeke, M. R.: Improving the Representation of Polar Snow and Firn in the Community Earth System Model, Journal of Advances in Modeling Earth Systems, 9, 2583–2600, https://doi.org/10.1002/2017MS000988, 2017.

Vionnet, V., Brun, E., Morin, S., Boone, A., Faroux, S., Moigne, P. L., Martin, E., and Willemet, J. M.: The detailed snowpack scheme Crocus and its implementation in SURFEX v7.2, Geoscientific Model Development, 5, 773–791, https://doi.org/10.5194/gmd-5-773-2012, 2012.

Waser, L. T., Ginzler, C., and Rehush, N.: Wall-to-Wall tree type mapping from countrywide airborne remote sensing surveys, Remote Sensing, 9, https://doi.org/10.3390/rs9080766, 2017.

Wieder, W. R., Lawrence, D. M., Fisher, R. A., Bonan, G. B., Cheng, S. J., Goodale, C. L., Grandy, A. S., Koven, C. D., Lombardozzi, D. L., Oleson, K. W., and Thomas, R. Q.: Beyond Static Benchmarking: Using Experimental Manipulations to Evaluate Land Model Assumptions, Global Biogeochemical Cycles, 33, 1289–1309, https://doi.org/10.1029/2018GB006141, 2019.

Xie, J., Jonas, T., Rixen, C., de Jong, R., Garonna, I., Notarnicola, C., Asam, S., Schaepman, M. E., and Kneubühler, M.: Land surface phenology and greenness in Alpine grasslands driven by seasonal snow and meteorological factors, Science of the Total Environment, 725, https://doi.org/10.1016/j.scitotenv.2020.138380, 2020.

Yuan, K., Zhu, Q., Zheng, S., Zhao, L., Chen, M., Riley, W. J., Cai, X., Ma, H., Li, F., Wu, H., and Chen, L.: Deforestation reshapes land-surface energy-flux partitioning, Environmental Research Letters, 16, https://doi.org/10.1088/1748-9326/abd8f9, 2021.

Yuan, K., Zhu, Q., Riley, W. J., Li, F., and Wu, H.: Understanding and reducing the uncertainties of land surface energy flux partitioning within CMIP6 land models, Agricultural and Forest Meteorology, 319, https://doi.org/10.1016/j.agrformet.2022.108920, 2022.

Zhang, T.: Influence of the seasonal snow cover on the ground thermal regime: an overview, Rev. Geophys., 43, 1–5, https://doi.org/doi:10.1029/2004RG000157, 2005.

Zhang, X., Wang, J., Gao, F., Liu, Y., Schaaf, C., Friedl, M., Yu, Y., Jayavelu, S., Gray, J., Liu, L., Yan, D., and Henebry, G. M.: Exploration of scaling effects on coarse resolution land surface phenology, Remote Sensing of Environment, 190, 318–330, https://doi.org/10.1016/j.rse.2017.01.001, 2017.

Zhuang, J., raphael dussin, Huard, D., Bourgault, P., Banihirwe, A., Raynaud, S., Malevich, B., Schupfner, M., Filipe, Levang, S., Jüling, A., Almansi, M., RichardScottOZ, RondeauG, Rasp, S., Smith, T. J., Stachelek, J., Plough, M., Pierre, Bell, R., and Li, X.: pangeo-data/xESMF: v0.7.1, https://doi.org/10.5281/ZENODO.7800141, 2023.

Zscheischler, J., Westra, S., Hurk, B. J. V. D., Seneviratne, S. I., Ward, P. J., Pitman, A., Aghakouchak, A., Bresch, D. N., Leonard, M., Wahl, T., and Zhang, X.: Future climate risk from compound events, Nature Climate Change, 8, 469–477, https://doi.org/10.1038/s41558-018-0156-3, 2018.